

# Effect of tau neutrino contribution to muon signals at neutrino factories

D. Indumathi and Nita Sinha  
*The Institute of Mathematical Sciences,  
Chennai 600 113, India.*

(Dated: October 8, 2018)

## Abstract

We discuss precision measurements of the leading atmospheric parameters at a standard neutrino factory with a detector that is sensitive to muons alone. The oscillation of the muon- and electron neutrinos in the neutrino factory beam to tau neutrinos adds to the muon events sample (both right sign and wrong sign) via leptonic decays of the taus produced through charge-current interactions in the detector. In particular, we study how this affects a precision measurement of the atmospheric mixing parameters and the deviation of  $\nu_\mu \leftrightarrow \nu_\tau$  mixing from maximality. In spite of the enhancement of the number of events due to the additional tau contribution, the determination of the atmospheric mixing angle and the deviation from maximality will be poorer. We show that it is impossible to devise satisfactory cuts to remove this tau contamination. Neglect of these tau contributions will lead to an incorrect conclusion about the precision obtainable at a neutrino factory.

PACS numbers: 14.60.Pq, 96.40.Tv, 95.55.Vj

## I. INTRODUCTION

Neutrino oscillations [1] are now well-established. The relevant mass-squared differences and mixing angles have also been studied in various experiments [2–6]; the study of neutrino oscillation physics is now at the precision stage with many existing and proposed near-future experiments. A natural progression in the precision study is to probe oscillation physics with neutrino factory beams.

In a neutrino factory, a  $\mu^+$  or  $\mu^-$  beam from a storage ring decays down a long straight section of the beam-line that points at a far-end detector. The decay of the muons produces a spectrum of electron and muon neutrinos via  $\mu^+ \rightarrow \bar{\nu}_\mu e^+ \nu_e$  and  $\mu^- \rightarrow \nu_\mu e^- \bar{\nu}_e$ , that is extremely well-understood. Charged-current (CC) interactions of the muon anti-neutrinos (neutrinos) in the detector lead to the production of  $\mu^+$  ( $\mu^-$ ) leptons. The electron neutrinos (anti-neutrinos), on the other hand, can *oscillate* into muon neutrinos (anti-neutrinos) which in CC interactions in the detector, produce  $\mu^-$  ( $\mu^+$ ) leptons, or muons with charge opposite to that from the unoscillated case and hence get detected as “wrong sign” (WS) muons.

In general, the focus of studies [7, 8] with neutrino factories (and the many papers and effort towards specifying the parameters of such a future neutrino factory) has been to pin down the as-yet unknown neutrino oscillation parameters, in particular, the across-generation 13 mixing angle  $\theta_{13}$  and the CP violating phase  $\delta_{CP}$ , in addition to other possibilities such as the mass hierarchy (or mass ordering in the 23 sector) and the octant of the 23 mixing angle  $\theta_{23}$  (whether it is larger or smaller than  $\pi/4$ ). All these can be best studied through measuring the WS events, as discussed above, in detectors capable of charge identification. The so-called right-sign (RS) (having the same charge as unoscillated) muon events are useful for precision measurements of the leading atmospheric parameters  $\theta_{23}$  and the atmospheric mass squared difference,  $\Delta m^2$ , apart from their use in understanding cross-section and flux uncertainties. In particular, they are sensitive probes of whether  $\nu_\mu \leftrightarrow \nu_\tau$  mixing is maximal, when  $\theta_{23} = \pi/4$ ; we shall refer to this value of  $\theta_{23}$  as being maximal. Such maximal mixing usually arises from an underlying symmetry [9] that would dictate the structure of the neutrino mixing matrix. Measurement of deviation from maximality is therefore of great significance in developing models for neutrino masses and mixings.

In this paper, we address the little-studied issue of contamination of the (right or wrong sign) muon events sample from oscillations of the muon or electron neutrinos or anti-neutrinos to tau neutrinos or anti-neutrinos, which, through CC interactions in the detector, result in tau leptons that subsequently decay to muons. While tau-production in neutrino-nucleus collisions has been studied in great detail, for example in Ref. [10], there are not many studies on the implications of the tau contamination (through leptonic decay) of the CC muon or electron events.

Tau contributions naturally arise in multi-GeV CC neutrino–nucleus interactions. Although the tau CC events are kinematically suppressed due to the large tau mass,  $m_\tau = 1.78$  GeV, the total contribution from taus is substantial since  $\nu_\mu \leftrightarrow \nu_\tau$  oscillations are large, being driven by a nearly maximal  $\theta_{23}$ . Here we focus on how this contribution affects a precision measurement of the deviation of  $\nu_\mu \leftrightarrow \nu_\tau$  mixing from maximal, i.e., a precision measurement of  $\theta_{23}$  and its deviation from maximal.

Tau contributions enhance both the RS and WS event rates in both the muon and electron sectors, since the leptonic tau decay fraction into both electrons and muons is about the same ( $\approx 17\%$ ). In particular, we find that tau contributions substantially enhance the *right-sign* muon event rates, especially at small final lepton energies, *independent of*  $\theta_{13}$ . However, due to a different parameter dependence, the tau contribution to muons *worsens* the determination of the deviation from maximality of  $\theta_{23}$  while leaving the determination of

$|\Delta m^2|$  unchanged. We also show that it is practically impossible to devise satisfactory cuts to remove this tau contamination. Hence, studies (beyond those discussed here) at neutrino factories must first bring the relatively little-studied uncertainties due to tau production and decay under control in order to achieve the expected precision measurements with muon detection.

The paper is organized as follows. In the next section, we briefly describe the physics of neutrino oscillations as is relevant for this study. We also list here the current limits on the oscillation parameters. In Section 3, we discuss the inputs such as the neutrino fluxes and cross-sections and preferred base-lengths. While we use standard packages for the deep inelastic scattering (DIS) cross-sections involving muon neutrinos, we use the mass-corrected leading order (LO) expressions for the tau contributions as discussed in Ref. [10], as well as comment on the next-to-leading order (NLO) contributions. In Section 4, we calculate numerically the event rates for various processes at an iron calorimeter detector capable of detecting muons with charge identification, such as the proposed ICAL/INO or the numerically mooted MIND. The numerical computation involves the calculation of the neutrino factory fluxes, the probability amplitudes using a solver for the neutrino evolution equation, which has been described in Ref. [11], calculation of the double differential cross section and in addition, the differential decay rate of the taus to muons, in case of the tau contribution. We conclude in Section 5.

## II. OSCILLATION PROBABILITIES

With a long baseline, the large matter effects in the course of neutrino propagation help in improved sensitivity to many parameters. In general, the 3-flavor probabilities,  $P_{ij}$ , of flavor  $\nu_i$  oscillating into flavor  $\nu_j$ , depend on all the oscillation parameters (in vacuum): the mixing angles  $\theta_{ij}$ ,  $i, j = 1, 2, 3$ , the CP violating phase,  $\delta_{CP}$  and the mass-squared differences  $\Delta_{ij} = m_i^2 - m_j^2$ , as well as the density of Earth's matter. The following analytic expressions [12] for these probabilities for neutrino propagation in earth matter in the constant density approximation, are useful to qualitatively exhibit the parameter dependence and for understanding the exact numerical results of the next section:

$$\begin{aligned}
P_{e\mu} &\approx \sin^2 \theta_{23} \sin^2 2\theta_{13}^m \sin^2 \Delta_{31}^m, \\
P_{e\tau}^m &\approx \cos^2 \theta_{23} \sin^2 2\theta_{13}^m \sin^2 \Delta_{31}^m, \\
P_{\mu\mu}^m &\approx 1 - \sin^2 2\theta_{23} \left[ \sin^2 \theta_{13}^m \sin^2 \Delta_{21}^m + \cos^2 \theta_{13}^m \sin^2 \Delta_{32}^m \right] - \sin^4 \theta_{23} \sin^2 2\theta_{13}^m \sin^2 \Delta_{31}^m, \\
P_{\mu\tau}^m &\approx \sin^2 2\theta_{23} \left[ \cos^2 \theta_{13}^m \sin^2 \Delta_{32}^m - \cos^2 \theta_{13}^m \sin^2 \theta_{13}^m \sin^2 \Delta_{31}^m + \sin^2 \theta_{13}^m \sin^2 \Delta_{21}^m \right], \quad (1)
\end{aligned}$$

where terms involving solar mass terms have been ignored [13] and the superscript  $m$  refers to mixing angles and mass square differences in matter.

For the atmospheric mass squared difference we use the notation [14]  $\Delta m^2 \equiv m_3^2 - \frac{1}{2}(m_1^2 + m_2^2)$ , so that a normal or inverted hierarchy is simply indicated by a sign (and not magnitude) change in this parameter.

We use a Runge-Kutta solver to calculate the oscillation probabilities for various energies and path lengths. Some technical details are given in Ref. [11]. All numerical results presented in this paper have been obtained using the density profile of the Earth as given by the Preliminary Reference Earth Model (PREM) [15] and numerically evolving the flavor eigenstates through Earth's matter. In particular, the approximate expressions for the probabilities as shown in Eq. (1) are not used.

Parameter	Best-fit value	2- $\sigma$ error
$\Delta_{21}[10^{-5}] \text{ eV}^2$	$7.65^{+0.23}_{-0.20}$	7.25–8.11
$ \Delta m^2  [10^{-3}] \text{ eV}^2$	$2.40^{+0.12}_{-0.11}$	2.18–2.64
$\sin^2 \theta_{12}; [\theta_{12}]$	$0.304^{+0.022}_{-0.016}; [33.5^\circ]$	0.27–0.35
$\sin^2 \theta_{13}; [\theta_{13}]$	$0.01^{+0.016}_{-0.011}$	$< 0.040; [11.5^\circ]$
$\sin^2 \theta_{23}; [\theta_{23}]$	$0.50^{+0.07}_{-0.06}; [45.0^\circ]$	0.39–0.63

TABLE I: Table showing currently accepted [16] best-fit values of oscillation parameters with  $2\sigma$  errors. In the case of the mixing angle  $\theta_{13}$ , a  $2\sigma$  upper bound is shown.

### A. Existing constraints on the oscillation parameters

The currently accepted [16] best-fit values of the oscillation parameters are summarized in Table I. The sign of the mass-squared difference  $\Delta m^2$  as well as any possible deviation of  $\theta_{23}$  from maximality (as well as its octant) are not yet determined. Also, there exists just an upper bound on the effective (13) mixing angle, while the CP violating phase  $\delta_{CP}$  is unknown.

Here, we will focus on precision measurement of deviation of  $\theta_{23}$  from maximality, i.e., deviation from  $\pi/4$ . We base the detector near the magic base-line, at  $L = 7,400$  km, so that the results are insensitive to the unknown  $\delta_{CP}$ . We will assume that a combination of solar neutrino experiments and the KamLAND reactor[2, 4] experiment completely determines the parameters  $\Delta_{21}$  and  $\theta_{12}$ . Since these play an insignificant role in determination of the atmospheric parameters, we set them to the best-fit values given in Table I and do not vary them in this analysis.

### B. Tau contributions and $\theta_{23}$

The  $\nu_\mu \leftrightarrow \nu_\tau$  oscillations are large, being driven by a nearly maximal  $\theta_{23}$ . Furthermore, as seen from Eq. (1),  $P_{\mu\tau}$  remains large even if  $\theta_{13}$  vanishes. Although there is kinematic suppression of the CC cross-section for tau production due to the large tau mass and the decay rate into electrons and muons is about 17%, there is still a sizeable tau production rate, which feeds into the muon production rate upon leptonic tau decay. In particular, this adds to the *right sign* muon event rate, and can even double it at low muon energies, since the tau decays preferentially produce low energy muons. It should therefore be taken into account in a precision analysis.

On the other hand, as seen from the same equation,  $P_{e\tau}$  is proportional to powers of  $\sin \theta_{13}$  and the tau contribution to WS muons is therefore small. It is of course comparable to the direct (from  $\nu_e$ ) wrong sign muon production rate to which it adds, although rather smaller since the large tau mass suppresses the cross-section; in addition, the contributing events are from further decay of the tau into muons and hence the rate is further suppressed. While the analysis of wrong sign muon events to determine parameters such as  $\theta_{13}$ , CP phase, etc., should perhaps include this contribution, it will have a negligible effect on the analysis at hand, viz., deviation of  $\theta_{23}$  from maximality; however, in our numerical analysis we do include this contribution.

In short, tau contribution to muon events from  $\nu_\mu \leftrightarrow \nu_\tau$  oscillations is large and adds to the right sign events; its contribution from  $\nu_e \leftrightarrow \nu_\tau$  oscillations is small and adds to the wrong sign events. Hence there are additional muon events from  $\nu_\tau$  in both RS and WS sectors to the direct events arising from (oscillated or unoscillated)  $\nu_\mu$  interactions.

*a. RS Events* : The RS events are not very sensitive to the octant of  $\theta_{23}$ . Notice that two of the terms of  $P_{\mu\mu}$  depend only on  $2\theta_{23}$  and are insensitive to the octant of  $\theta_{23}$ . Further, for small  $\theta_{13}$ , the octant dependent term in  $P_{\mu\mu}$  has negligible contribution, while  $P_{\mu\tau}$  is completely independent of the octant. Similarly, individually, both are sensitive to the *deviation* of  $\theta_{23}$  from maximality, but they have different dependences on this parameter.

To leading order in  $\theta_{13}$ ,  $P_{\mu\mu} \sim 1 - \sin^2 2\theta_{23} \cdot F$  while  $P_{\mu\tau} \sim \sin^2 2\theta_{23} \cdot F$ , where  $F = \sin^2 \Delta_{32}^m$ . Since the  $\theta_{23}$  dependent terms come with opposite sign, the combination of muons from direct production and from tau decays marginally decreases the sensitivity of the event rates to this angle (and its deviation from maximality). However, as we shall see later, it is almost impossible to remove the tau events. Any cuts that attempt to do so drastically reduce the direct muon events as well and hence worsen the sensitivity to the oscillation parameters. Thus, the combined contribution of events from direct muon production and those from tau decay is less sensitive to the deviation from maximality. Neglect of the tau contribution will lead to an incorrect conclusion about the precision possible for the deviation from maximality. This is the crux of our result.

*b. WS Events* : Notice that  $P_{e\mu}$  and  $P_{e\tau}$  are both sensitive to the octant of the 23 mixing angle,  $\theta_{23}$ , while their sum is less sensitive (indeed, the sum would be wholly independent of  $\theta_{23}$ , if one were to neglect the differences in the  $\nu_\mu$ -nucleon and  $\nu_\tau$ -nucleon cross-sections). Hence the tau contribution affects precision measurements in the WS sector as well.

Here we have focused on events with muons in the final state. However, taus also equally contribute to events with electrons in the final state. These events are interesting for other precision measurements and have been discussed in the context of  $\nu_\mu \rightarrow \nu_e$  appearance or the “platinum channel” where charge identification of electrons is also contemplated. Here the situation with respect to the tau contribution is drastically different. The tau contribution to electron events from  $\nu_\mu \leftrightarrow \nu_\tau$  oscillations (with subsequent decay of tau into electrons) is large and adds to the wrong sign events. Hence signatures in the “platinum channel” may suffer from these large additional contributions, independent of  $\theta_{13}$ . This platinum channel is well-motivated when  $\theta_{13}$  is large (when the “direct”, that is, not tau-generated, contribution is large); in such a case, the tau contamination from  $\nu_e \leftrightarrow \nu_\tau$  oscillations also turns on and becomes a small addition to the right sign electron events.

Hence the inclusion of tau leptonic decay boosts the signal for muon RS events and spoils the purity of the electron WS events. Details of this contribution to the electron events will be presented separately.

### III. THE INPUTS: FLUXES, KINEMATICS, CROSS-SECTIONS

#### A. The neutrino factory fluxes

We assume a basic muon storage ring configuration [17] with muon beam energy  $E_b = 25$  GeV, with  $5 \times 10^{20}$  useful decays per year. The muon antineutrino (neutrino) and electron neutrino (antineutrino) distributions for  $\mu^\pm$  decay in the muon rest frame are given by,

$$\begin{aligned} \frac{d^2 N_{\bar{\nu}_\mu, \nu_\mu}}{dx d\Omega} &\propto \frac{2x^2}{4\pi} [(3 - 2x) \mp (1 - 2x)P_\mu \cos \theta] , \\ \frac{d^2 N_{\nu_e, \bar{\nu}_e}}{dx d\Omega} &\propto \frac{12x^2}{4\pi} [(1 - x) \mp (1 - x)P_\mu \cos \theta] , \end{aligned}$$

where  $P_\mu$  is the average muon polarization along the beam direction,  $E_\nu$  denotes the neutrino energy,  $x = 2E_\nu/m_\mu$  and  $\theta$  is the angle between the neutrino momentum and muon spin

vector.

For unpolarized muon beams, in the laboratory frame the boosted flux distributions are given by,

$$\begin{aligned}\frac{d^2 N_{\nu_\mu}}{dy d\Omega_{\text{lab}}} &= \frac{4n_\mu}{\pi L^2 m_\mu^6} E_b^4 y^2 (1 - \beta \cos \varphi) \left[ 3m_\mu^2 - 4E_b^2 y (1 - \beta \cos \varphi) \right] , \\ \frac{d^2 N_{\nu_e}}{dy d\Omega_{\text{lab}}} &= \frac{24n_\mu}{\pi L^2 m_\mu^6} E_b^4 y^2 (1 - \beta \cos \varphi) \left[ m_\mu^2 - 2E_b^2 y (1 - \beta \cos \varphi) \right] ,\end{aligned}$$

where  $y = E_\nu/E_b$ ,  $n_\mu$  is the number of useful muons per year,  $L$  is the base-line distance from source to detector, and  $\varphi$  is the angle between the beam axis and the direction to the detector (which is assumed to be the forward or  $z$ -direction).

In general, the decaying muon beam has a finite divergence ( $\sim mr$  or less) so that it has an angular spread about the central beam direction. Further, the neutrinos are emitted in a forward cone that becomes narrower as  $E_b$  increases. We can relate the neutrino–muon opening angle  $\varphi$  to the angles  $\alpha$  (muon direction with respect to the  $z$ -axis) and  $(\theta', \phi')$  (neutrino direction with respect to the  $z$ -axis) as,

$$\cos \varphi = \cos \alpha \cos \theta' + \sin \alpha \sin \theta' \cos \phi' .$$

The neutrino fluxes can be (analytically) integrated over the muon beam angle  $\alpha$ , assuming a gaussian angular divergence of the muon beam around the  $z$ -axis with standard deviation taken to be [18]  $\sigma = 0.1/\gamma$ , with the usual definition of  $\gamma = E_b/m_\mu$ . The resulting neutrino flux is a function of  $(\theta', \phi')$  alone. A trivial integration over  $\phi'$  thus gives the neutrino fluxes as a function of the neutrino angle,  $\theta'$ . The kinematic boost ensures that about half of the neutrinos are emitted within a cone  $\theta' \leq 1/\gamma$ . Even though the opening angle is very small, notice that the flux is not uniform in  $\theta'$ ; this can be important especially to understand the fluxes at near detectors as well as its spread at the detector. We average the forward flux over a small angle  $\theta' < \epsilon = 0.3\sigma$  where the intensity is fairly flat as a function of distance from the central axis to obtain the energy spectrum  $dN/dE_\nu$  of the electron and muon neutrinos. This corresponds to knowing the neutrino beam direction to a precision of roughly 0.1 mr.

The resulting neutrino spectrum with gaussian angular spread averaged over  $(\theta' < \epsilon, 0 \leq \phi' \leq 2\pi)$  is

$$\begin{aligned}\frac{dN_\mu}{dE_\nu} &\equiv \frac{1}{E_b} \frac{1}{\int d\Omega} \int d\Omega \left\langle \frac{dN_\mu}{dy d\Omega} \right\rangle_G = \frac{4n_\mu \gamma^4 y^2}{\pi L^2 E_b} \left\{ 3 - 4y\gamma^2 - \frac{\beta}{2} (3 - 8y\gamma^2) (1 + c_\epsilon) e^{-\sigma^2/2} \right. \\ &\quad \left. - \frac{1}{3} y (\gamma^2 - 1) [4 + c_\epsilon + c_\epsilon^2 + e^{-2\sigma^2} 3c_\epsilon (1 + c_\epsilon)] \right\} , \\ \frac{dN_e}{dE_\nu} &\equiv \frac{1}{E_b} \frac{1}{\int d\Omega} \int d\Omega \left\langle \frac{dN_e}{dy d\Omega} \right\rangle_G = \frac{24n_\mu \gamma^4 y^2}{\pi L^2 E_b} \left\{ 1 - 2y\gamma^2 - \frac{\beta}{2} (1 - 4y\gamma^2) (1 + c_\epsilon) e^{-\sigma^2/2} \right. \\ &\quad \left. - \frac{1}{6} y (\gamma^2 - 1) [4 + c_\epsilon + c_\epsilon^2 + e^{-2\sigma^2} 3c_\epsilon (1 + c_\epsilon)] \right\} , \quad (2)\end{aligned}$$

where  $c_\epsilon, s_\epsilon$  refer to  $\cos \epsilon, \sin \epsilon$ . The (unoscillated) neutrino spectrum at a detector  $L = 7,400$  km away is shown in Fig. 1. The neutrino and anti-neutrino spectrum of the same flavor (from muon beams of opposite charge) are the same if the muon mass is neglected, as has been assumed here.

Note that, in the absence of oscillations, the number of events in the neutrino sector is always a factor of two or more larger than in the case of anti-neutrinos due to the larger

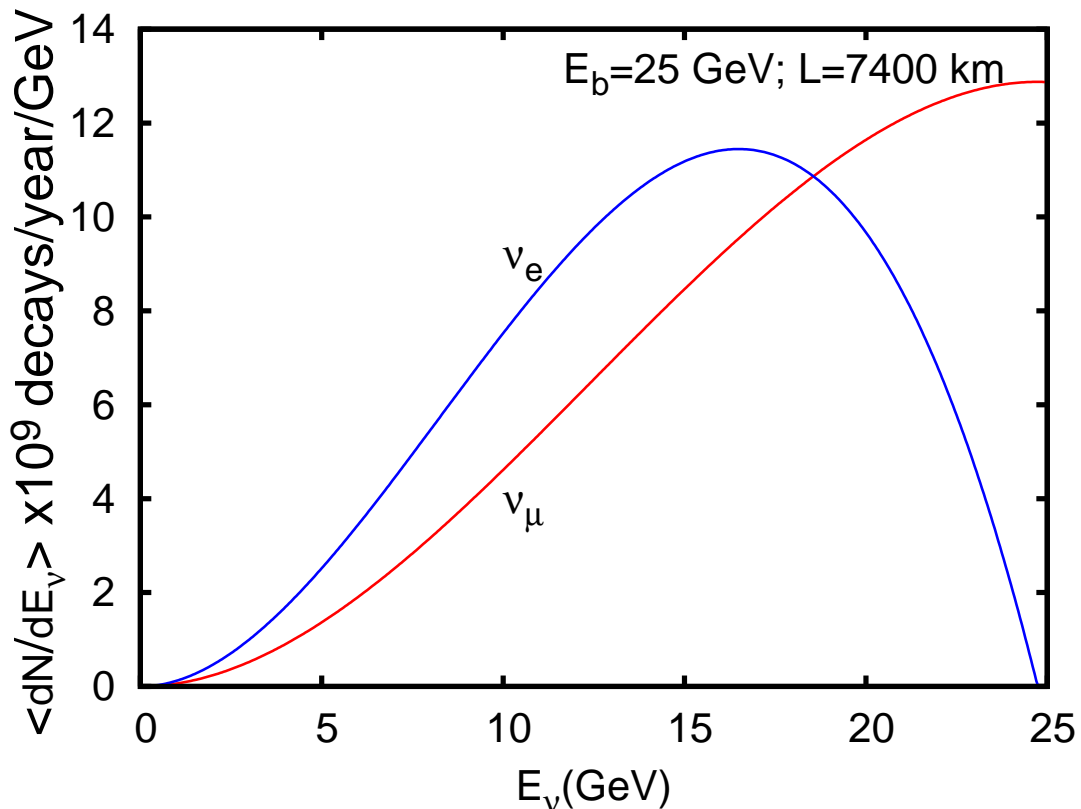


FIG. 1: Unoscillated electron and mu neutrino spectrum from a muon factory at a distance of  $L = 7,400$  km, with  $E_b = 25$  GeV muons.

neutrino cross-section. Hence, studies of wrong-sign muons tend to focus on  $\mu^+$  beams where the wrong sign events correspond to  $\mu^-$  from neutrino–nucleus interactions. Here, we are interested in the right sign events, and so would prefer  $\mu^-$  factory beams; however, we sum over events from both  $\mu^-$  and  $\mu^+$  beams, assuming an equal (and simultaneous) running time of 5 years in each case.

## B. The kinematics

We are interested in processes that yield muons (of either charge) in the final state. These arise from CC interactions in which either muons or taus are produced, with the latter decaying into muons. Studies with neutrino factory beams typically use integrated cross-sections and aim at reconstructing the initial neutrino energy and direction; here we focus on the spectrum of the final state muon and hence require the detailed kinematics of the interactions, both for direct muon production and via tau decay.

In the laboratory frame, a neutrino of flavor  $l = \mu$  or  $\tau$  and energy  $E_\nu$  interacts with a nucleon of mass  $M$  and produces the corresponding charged lepton  $l$  at an angle  $\theta_l$  w.r.t. the incident neutrino direction, which we take to be the  $z$ -axis. In the case of  $\nu_\tau$  interactions, the azimuthal angle of the muon from tau decay,  $\phi_\mu$ , is also relevant: the tau is produced at a very forward angle while  $\phi_\mu$  is restricted by the decay kinematics. The available phase space is restricted in both direct muon and tau production due to the constraint on the available

energy for the lepton:  $E_- < E_l < E_+$ ; see Appendix A for the detailed expressions on the constraints.

The effect of this pinching in available energy, for the case of a  $\tau$  lepton being produced, can be seen in Fig. 2 where the final hadronic mass  $m_X$  is plotted as a function of  $E_\tau$ . The notation is standard:  $m_X^2 = W^2 = (p + q)^2$ , where  $p, q$  are the nucleon and the intermediate gauge boson 4-momenta in the laboratory frame.

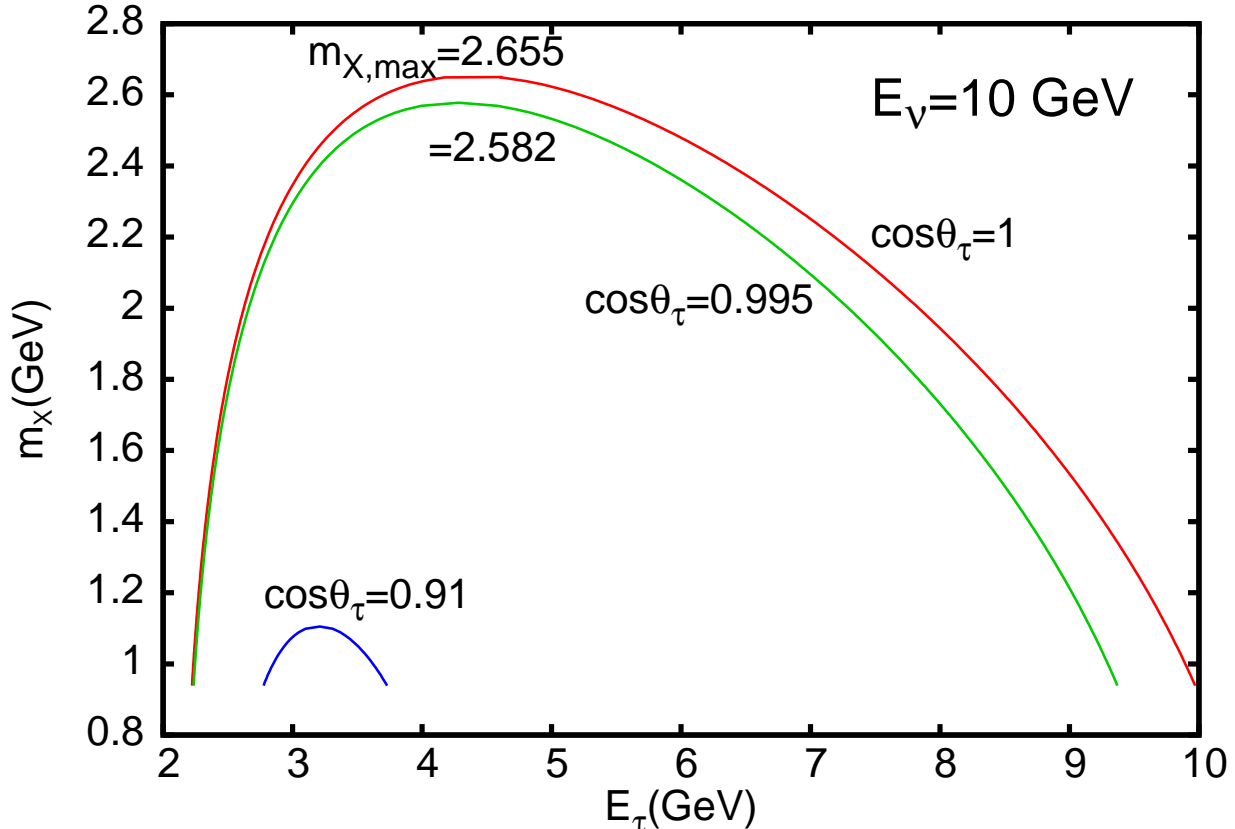


FIG. 2: Kinematics of  $\nu_\tau$ -nucleon CC interactions. The figure shows the allowed parabolas of constant  $\cos\theta_\tau$  in the  $m_X$ - $E_\tau$  plane for  $E_\nu = 10$  GeV. The ends of the parabolas (at  $m_X = m_{X,\min} = M$ ) give the limits of the allowed tau lepton energy, which are severely restricted for  $\cos\theta_\tau$  away from 1.

The allowed tau energy limits  $E_\pm$  for a given  $\cos\theta_\tau$  correspond to the end points of the parabola in the  $m_X$ - $E_\tau$  plane. For example, for a typical neutrino energy  $E_\nu = 10$  GeV, there is hardly any allowed energy region for  $\cos\theta_\tau = 0.91$ . Hence, the tau leptons are produced in a very forward direction while the direct muons, due to their lighter mass, are less restricted.

### C. The cross-sections

Since the energies of interest range from a few GeV to 25 GeV, the CC interactions include quasi-elastic (QE), resonance (Res) and deep inelastic (DIS) processes.

Unlike many other calculations, we consider not the total but the double differential cross-sections for muon production with detailed energy and direction information so that



we have better control on the spreads in the muon energy and direction. Use of total cross-sections requires the reconstruction of the original neutrino kinematics and introduces larger errors due to large uncertainties in reconstruction of the associated hadron kinematics. The differential cross-section may be written in the form,

$$\frac{d\sigma}{dE_l d\cos\theta_l} = \frac{G_F^2 \kappa^2}{2\pi} \frac{p_l}{M} \left\{ \sum_{i=1}^5 a_i W_i \right\}, \quad (3)$$

where  $G_F$  is the Fermi constant,  $\kappa = M_W^2/(Q^2 + M_W^2)$  is the propagator factor with the  $W$  boson mass,  $M_W$ ,  $p_l$  is the magnitude of three-momentum of the charged lepton and the  $W_i$  are structure functions corresponding to the general decomposition of the hadronic tensor for QE, Res and DIS processes. We have

$$\begin{aligned} \sum_{i=1}^5 a_i W_i &= \left( 2W_1 + \frac{m_l^2}{M^2} W_4 \right) (E_l - p_l \cos\theta_l) + W_2 (E_l + p_l \cos\theta_l) \\ &\pm \frac{W_3}{M} (E_\nu E_l + p_l^2 - (E_\nu + E_l) p_l \cos\theta_l) - \frac{m_l^2}{M} W_5. \end{aligned} \quad (4)$$

The detailed expressions for  $W_i$  are taken from Ref. [10] where the specific structure functions are listed for QE, Res and DIS leading order (LO) processes. A few comments are in order.

The  $W_1$  and  $W_2$  functions are those that appear in neutral current (NC) lepton-nucleon scattering processes as well, while  $W_3$  is a signature of the parity violating nature of weak interactions. The structure functions  $W_4$  and  $W_5$  only appear when the mass of the charged lepton is taken into account. For consistency, we use non-zero masses for both muon and tau leptons in the calculation; however,  $W_4$  and  $W_5$  are actually relevant only for the heavy tau.

The quasi-elastic events dominate at lower energies. The separation between Res and DIS is arbitrary and determined by a cut, chosen to be  $W > W_{\text{cut}} = 1.4$  GeV. This still leaves  $Q^2 \equiv -q^2$  undetermined. However, reliable perturbative estimates for DIS can only be made when  $Q^2 > \text{few GeV}^2$ . A few percent of the events satisfy the cut on  $W$  for DIS but have very low  $Q^2$  (and hence very small values of the Bjorken scaling variable,  $x = Q^2/(2p \cdot q)$ ), thus making cross-section estimates for these cases extremely uncertain. Removing these events will lead to an underestimate of the actual number of DIS events; estimating them by scaling their  $Q^2$  to  $Q_{\text{min}}^2 \sim 2$  GeV<sup>2</sup> overestimates the cross-sections since the structure functions are large when  $x$  is small.

For both mu and tau interactions we use the CTEQ6 LO set of parton distribution functions. In this parameterization set, the starting value is  $Q_0 = 1.3$  GeV, or the charm mass. Since backwards evolution is unstable, the problem lies with events with  $Q^2 < Q_0^2 = 1.69$  GeV<sup>2</sup>.

The effect of either choice (removing the event or adding it by estimating its contribution at a larger  $Q^2$ ) is shown in Fig. 3 for both mu and tau interactions. In choice  $c_1$ , for all events with  $Q^2 < Q_0^2$ , the parton distributions are estimated with  $Q^2 = Q_0^2$ , while  $\alpha_s$  and  $x$  are kept at their true values. Hence this choice overestimates the event rate. In choice  $c_3$ , all such events are thrown away, so this choice underestimates the event rate.

The ‘‘true’’ cross-section would probably lie between the two extreme estimates and is probably close to the cross-section with choice  $c_2$ , where events with  $Q^2 < 1$  GeV<sup>2</sup> are thrown away, while for events with  $1 < Q^2 < Q_0^2$ , the parton distributions are computed with  $Q^2$  rescaled to  $Q_0^2$ .

Notice that the uncertainties are larger for the mu case (and also will be large for the electron case) and is less severe for the tau.

It should also be noted that this issue of perturbative tractability cannot be cured by going to higher orders in the calculation. For instance, the effect of including NLO contributions to the DIS cross-section in the  $c_1$  case in the limit of massless quarks and target hadrons is also shown in Fig. 3. The parton distribution functions are again from the CTEQ6 NLO set while the coefficient functions are given in Ref. [19]. While this is correct for the muon case, there are further mass corrections for tau interactions [20, 21] which are severe since they lead to effective higher twist terms. A discussion of these corrections can be found in Ref. [21]; however, the uncertainty from the small- $Q^2$  events overwhelms the changes in going from LO to NLO. For the numerical calculations that follow, therefore, we use the LO expressions throughout, which are correct (including mass corrections) for both muon and tau interactions.

Actual measurements at low and medium  $Q^2$  are essential to close this gap in our understanding of neutrino–nucleon cross-sections. This may be possible in the near future with measurements from MINOS, Minerva, T2K, Argoneut, etc. [22].

In summary, we use the CTEQ6 LO parton distribution set throughout this paper, with choice  $c_1$ . The quasi-elastic, resonance and DIS total cross-sections for  $\nu_\mu$  and  $\nu_\tau$  (and their anti-particle)–nucleon CC interactions are shown in Fig. 4. The lower (upper) curve corresponds to interaction of the (anti)-neutrino with an isoscalar nucleon (average of proton and neutron). The actual numerical calculations use the differential cross-sections shown in Eq. (3).

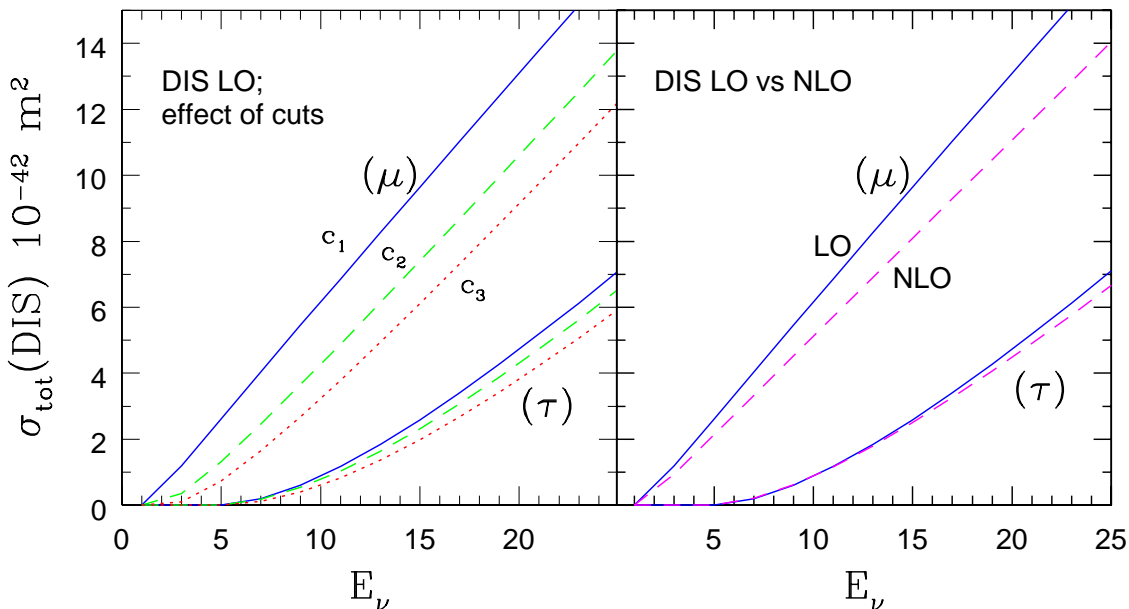


FIG. 3: Total deep inelastic scattering (DIS) CC  $\nu_\tau$ –nucleon cross-section as a function of the neutrino energy. The left figure shows the impact of different cuts on the cross-section. See text for details. The right figure shows the effect of including NLO effects to the  $c_1$  curve. The upper set of curves is for mu (or electron) DIS; the lower ones for tau.

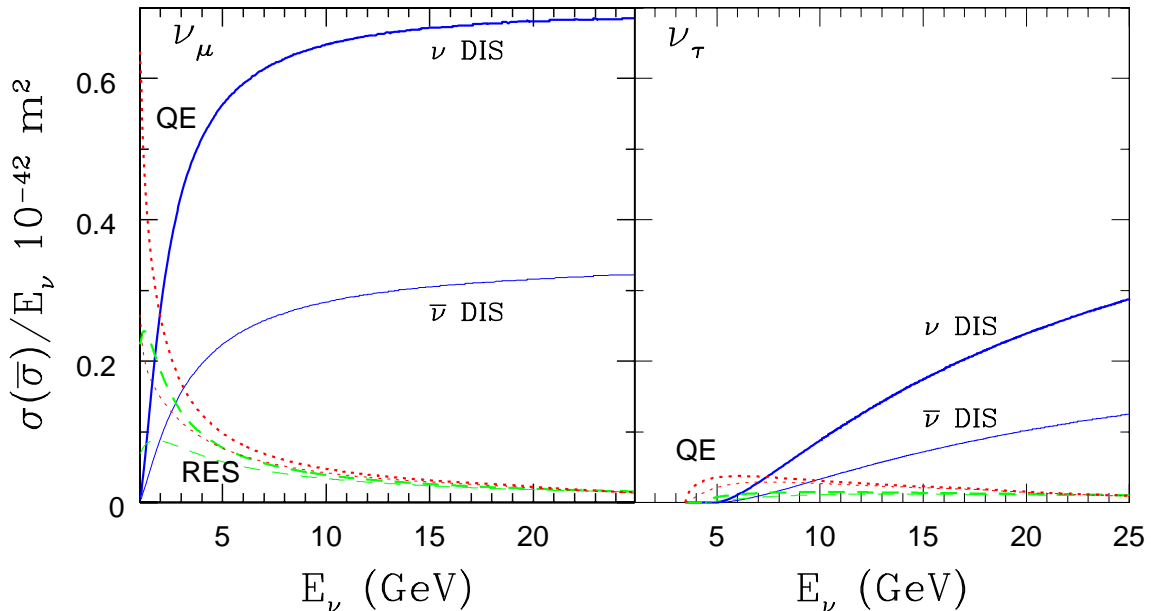


FIG. 4: Total quasi-elastic, resonance and deep inelastic scattering (DIS) CC (anti)neutrino-nucleon cross-section as a function of the neutrino energy for  $\nu_\mu$  and  $\nu_\tau$  interactions.

#### D. Tau decay

Here we focus on the leptonic decay mode of the tau, for example  $\tau^- \rightarrow \nu_\tau \mu^- \bar{\nu}_\mu$ , where the final muon from tau decay adds to the direct muon signal from  $\nu_\mu$ -nucleon CC interactions. While the branching fraction into muons (or electrons) is about 17%, we are again interested in the detailed kinematics of the final state muon and hence use the differential decay rates; see Appendix A for details.

The typical decay rate for a tau with energy  $E_\tau = 10$  GeV is shown as a function of the muon energy and direction (with respect to that of the parent tau) in Fig. 5. Notice that the muon is emitted mostly in the direction of the tau (which was itself forwardly peaked) while its energy is typically highly degraded compared to its parent. Hence, muons produced in  $\nu_\tau$  interactions mostly contribute to the *forward event rate at low energy*. The fractional decay rate has been plotted so that the area under the curve in both cases is 17%.

## IV. EVENT RATES IN A FAR-DETECTOR

### A. Preliminaries

We assume that the neutrinos interact with a 50 kton iron detector such as the proposed INO/ICAL or MIND detector. Both  $\mu^+$  and  $\mu^-$  beams are considered, with equal exposure for each. There are two kinds of contributions in the signal:

1. The “direct” muons arising from CC interactions of muon neutrinos (or anti-neutrinos) on the target.
2. The “tau-induced” muons arising from CC interactions of tau neutrinos (or anti-neutrinos) on the target, with the subsequent decay of the produced taus into muons.

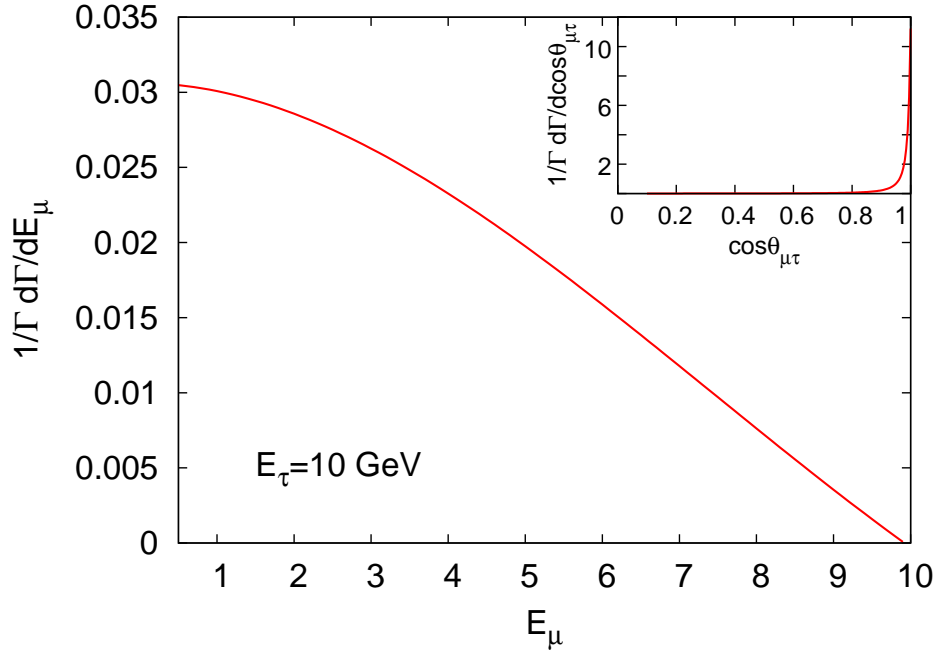


FIG. 5: Tau decay rate as a function of the final muon energy  $E_\mu$  and direction (inset) for tau with energy  $E_\tau = 10$  GeV. Here  $\theta_{\mu\tau}$  is the opening angle between the muon and its parent tau.

While the decay fraction is small, the tau events are large, as mentioned earlier, and hence this contribution is significant.

In addition, there are right sign (RS) and wrong sign (WS) events for each of these. Table II clarifies the nature of different sources of muons in the final state. The charge of the RS/WS lepton depends on the charge of the muon in the storage ring. However, we do not identify the charge of the final charged lepton: all muon events are simply added. This is because the RS events are sensitive to deviations from maximality of  $\theta_{23}$ ; the WS events are very small compared to the RS events and their inclusion may only marginally worsen the results; however, the advantage gained in being “charge-blind” is significant, especially in the errors.

Beam in Storage ring	Neutrinos in beam	RS muons		WS muons	
		Direct	Tau	Direct	Tau
$\mu^-$	$\nu_\mu$	$N_\mu \cdot P_{\mu\mu} \cdot \sigma_\mu$	$N_\mu \cdot P_{\mu\tau} \cdot \sigma_\tau \cdot \Gamma_\tau$	–	–
	$\bar{\nu}_e$	–	–	$\bar{N}_e \cdot \bar{P}_{e\mu} \cdot \bar{\sigma}_\mu$	$\bar{N}_e \cdot \bar{P}_{e\tau} \cdot \bar{\sigma}_\tau \cdot \Gamma_\tau$
$\mu^+$	$\bar{\nu}_\mu$	$\bar{N}_\mu \cdot \bar{P}_{\mu\mu} \cdot \bar{\sigma}_\mu$	$\bar{N}_\mu \cdot \bar{P}_{\mu\tau} \cdot \bar{\sigma}_\tau \cdot \Gamma_\tau$	–	–
	$\nu_e$	–	–	$N_e \cdot P_{e\mu} \cdot \sigma_\mu$	$N_e \cdot P_{e\tau} \cdot \sigma_\tau \cdot \Gamma_\tau$

TABLE II: The terms contributing to the production of right sign (RS) and wrong-sign (WS) muons from  $\nu_e$  and  $\nu_\mu$  neutrinos and anti-neutrinos with  $\mu^\pm$  beams in the storage ring. Negatively (positively) charged muons constitute the RS (WS) signal with neutrinos from a  $\mu^-$  storage ring and vice versa with  $\mu^+$  beams. Event rates are proportional to the product of the oscillation probabilities,  $P_{ij}$ , the neutrino fluxes,  $N_{e,\mu}$ , the differential CC cross-sections,  $\sigma_{\mu,\tau}$ , and the differential decay rate,  $\Gamma_\tau$  (in the case of  $\tau$ -induced muon production), as is symbolically shown.

The muon event rate is calculated as a function of the observed muon energy (and not that of the original neutrino that participated in the interaction). We have, generically, the number of muon events in a detector at a distance  $L$ ,

$$\begin{aligned}\mathcal{R}_{i,D}^b(E) &= K \int_{E_\nu^{\text{thr}}}^{E_\nu^{\text{max}}} dE_\nu \frac{dN_i(E_\nu, L)}{dE_\nu} \cdot P_{i\mu}(E_\nu, L) \int_0^1 d\cos\theta_\mu \int_{E_-}^{E_+} dE_\mu \frac{d\sigma_\mu(E_\nu, E_\mu, \theta_\mu)}{dE_\mu d\cos\theta_\mu} \cdot R(E_\mu, E), \\ \mathcal{R}_{i,\tau}^b(E) &= K \int_{E_\nu^{\text{thr}}}^{E_\nu^{\text{max}}} dE_\nu \frac{dN_i(E_\nu, L)}{dE_\nu} \cdot P_{i\tau}(E_\nu, L) \int_{c_{\text{min}}}^1 d\cos\theta_\tau \int_{E_-}^{E_+} dE_\tau \frac{d\sigma_\tau(E_\nu, E_\tau, \theta_\tau)}{dE_\tau d\cos\theta_\tau} \cdot \\ &\quad \int_{\text{restr.}} dE_\mu d\cos\theta_\mu d\phi_\mu \frac{1}{\Gamma_\tau} \frac{d\Gamma(E_\tau, E_\mu, \theta_\tau, \theta_\mu, \phi_\mu)}{dE_\mu d\cos\theta_\mu d\phi_\mu} \cdot R(E_\mu, E),\end{aligned}\quad (5)$$

where the superscript  $b$  refers to the beam-type,  $\mu^-$  or  $\mu^+$  circulating in the storage ring;  $i = \mu, \bar{e}(\bar{\mu}, e)$  denotes the neutrino type produced in a  $\mu^-(\mu^+)$  beam. Here  $K = N_t n_y$ ,  $N_t$  is the number of target nucleons (assumed isoscalar) and  $n_y$  is the number of years of data accumulation. The first expression in Eq. (5) corresponds to the production of direct muon (denoted by the subscript D) production while the second corresponds to  $\tau$  production with subsequent decay into muons (denoted by  $\tau$ ), with  $E$  being the observed energy of the muons.  $E_\nu^{\text{max}}$  is the maximum neutrino energy in the factory flux; the limits of integration are defined in Appendix A. Note that the integration over the final muon parameters, in case of tau production and decay, is restricted by an angular constraint; see Appendix A for details. The charge-blind events are obtained by summing over the index  $i$  and hence the total events for each beam are then obtained by the sum,

$$\mathcal{R}_{\text{tot}}^b(E) = \sum_i (\mathcal{R}_{i,D}^b(E) + \mathcal{R}_{i,\tau}^b(E)). \quad (6)$$

Due to finite detector resolution, the observed lepton energy  $E$  may not correspond to the true lepton energy. We assume that the muons are reconstructed with a gaussian resolution width of 7% ( $\sigma = 0.07E_\mu$ ) for energetic, GeV muons. (We focus on the charged muon distribution and do not try to reconstruct the energy and direction of the original neutrino.) This identifies  $R$  in Eq. (5) as the Gaussian energy resolution function of width  $\sigma$ .

We assume a 90% reconstruction efficiency of muons which is charge-independent, although we implicitly assume an iron calorimeter detector with charge identification capability as in the MINOS [23] and the proposed ICAL/INO [24] or simulated MIND detectors. We use the final muon (from direct muon production or via tau decay) event rates accumulated over five years, to study the sensitivity to the deviation of the mixing angle  $\theta_{23}$  from maximality.

## B. The event rates

At the magic [25] base-line,  $L = 7,400$  km, which is chosen here, there is no sensitivity to the CP phase  $\delta_{CP}$  which we henceforth set (arbitrarily) to zero. Typical event rates for the leading atmospheric parameters,  $\Delta m^2 = 2.4 \times 10^{-3}$  eV<sup>2</sup>,  $\theta_{23} = 42^\circ$  ( $\sin^2 2\theta_{23} = 0.9891$ ), the reactor angle  $\theta_{13} = 1^\circ$  ( $\sin^2 \theta_{13} = 0.0003$ ;  $\sin^2 2\theta_{13} = 0.0012$ ) and the solar parameters set to the central values given in Table I, are shown as a function of the observed charged lepton energy in Fig. 6. The panels show the direct muon production and tau decay contributions to the right sign (RS) and wrong sign (WS) observed muon events from  $\mu^-$  and  $\mu^+$  beams. Since the neutrino-nucleon cross-sections are larger than those for anti-neutrinos, the  $\mu^-$  ( $\mu^+$ ) beams have larger RS (WS) events. Hence,  $\mu^+$  beams are preferred for studying WS events (where charge identification is crucial) which are sensitive to non-zero  $\theta_{13}$ , 23 mass hierarchy, octant of  $\theta_{23}$  and the CP phase  $\delta$ , away from the

magic baseline. A  $\mu^-$  beam with larger RS events would be desirable for precision of  $\Delta m$  and  $\theta_{23}$ . However, using the full sample without charge identification is preferable, as the detection efficiency of the charge blind sample would be higher. Since the WS events are a small fraction of the large RS sample, using the sum does not worsen the precision of the parameters. We therefore add the events (RS+WS) from both  $\mu^-$  and  $\mu^+$  beams; the total event rate is also shown in the figure.

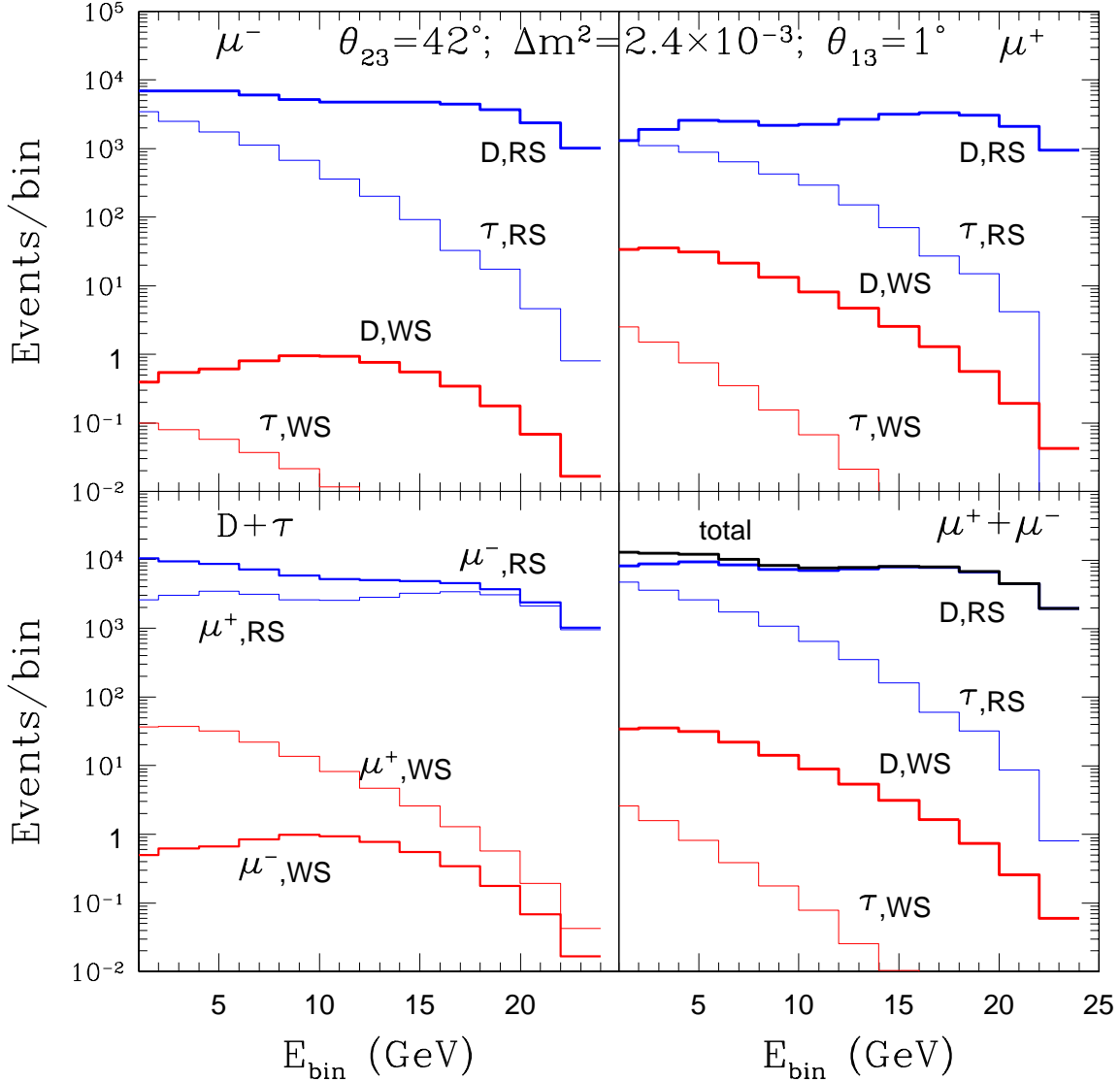


FIG. 6: Muon event rates over 5 years as a function of the observed muon energy, in bins of 2 GeV at a 50 kton muon detector distant  $L = 7,400$  km away from a muon factory neutrino source. Right sign (RS) and wrong sign (WS) events from  $\mu^-$  and  $\mu^+$  beams are shown in the upper panels. Contributions from direct muon production (denoted by  $D$ ) and that of muons from tau decay (labeled as  $\tau$ ) are separately shown. The left lower panel shows the sum  $D + \tau$ . Notice that there is a substantial contribution from tau decay to RS events, as seen in the right lower panel; also, the WS events have a negligible contribution to the total event rate. Oscillation parameters are as shown, with  $\Delta m^2$  in  $\text{eV}^2$  and other oscillation parameters as given in Table I.

It can be seen that there is a substantial contribution to the RS events from tau decay into muons. Since the tau life-time is very short, these events will add to the observed RS events from direct muon production in  $\nu_\mu$ -nucleon interactions. Since the tau contribution alters the sensitivity to the oscillation parameters as discussed in Section IIB and illustrated in Fig. 8, we next discuss whether these events can be removed through various cuts on the final charged lepton energy or production angle.

### C. Cuts on tau contribution

As stated earlier, tau production in neutrino-nucleon interactions is extremely forward-peaked; see Fig. 2. Furthermore, the muons produced in leptonic tau decay are also forward peaked; see Fig. 5. Hence, one obvious way to remove/reduce the tau contribution is an angular cut. Also, as can be seen from Fig. 5, the tau decay rate is large for muons produced with low energies, resulting in a substantial tau contribution to the muon events, at small observed muon energies (see Fig. 6). Hence, a muon energy cut can also be contemplated.

The effect of cuts on the event rates is seen in Fig. 7. The panels show the effect of an increasingly drastic angular cut on the final state muons. It can be seen that the only cut effective in removing/reducing the tau contribution is one (with  $\theta_\mu > 25^\circ$ ) that removes the signal itself! Alternately a muon energy cut, of about  $E > 10$ – $15$  GeV, can substantially remove the tau contribution, still leaving sufficient direct muons. However, such a large energy cut will worsen the precision to which the mixing parameters can be measured as sensitivity is higher in the lower energy bins where matter effects are larger. In short, it is not feasible to cut out the tau contribution and still make a precision measurement, in this case, of the deviation of  $\theta_{23}$  from maximality.

### D. Effect of the tau contribution

As stated earlier, the tau contribution alters the dependence on the mixing parameters, and thus alters the precision to which we can determine them. Fig. 8 shows the dependence of the direct and tau-induced muon events on  $\theta_{23}$ . While the tau events have less sensitivity to this parameter, the rate increases while the direct event rate decreases as  $\theta_{23}$  increases towards maximal  $\theta_{23} = \pi/4$ . However, the inclusion of muons from tau events alters the uncertainties considerably.

A look back at the expressions in Eq. (5) clearly shows a major difference between direct and total (including tau contribution) muon production that is most easily appreciated by explicitly writing out the dominant RS contribution in each case:

$$\begin{aligned} d\mathcal{R}_D^b(RS) &\sim P_{\mu\mu} dN_\mu d\sigma_\mu ; \\ d\mathcal{R}_\tau^b(RS) &\sim P_{\mu\tau} dN_\mu d\sigma_\tau d\Gamma_\tau . \end{aligned} \quad (7)$$

A near detector (where the oscillation probabilities are near zero and the survival probabilities are nearly 1), sensitive to muons, precisely measures the combination  $(dN_\mu d\sigma_\mu)$ , that is, flux times cross-section of the muons. This is what appears in the (RS) event rate for direct muon production and is therefore very well constrained from measurements at the near detector. Indeed, uncertainties are reduced to a factor of  $10^{-3}$ , mainly arising from differences in the shape of the flux at the near- and far-detectors.

However, what appears in the (RS) event rate expression via tau production and decay is the combination  $dN_\mu d\sigma_\tau$ . While the flux is the same as for direct muon production and in fact very well understood, the same is not true of the cross-section. While the muon cross-sections have

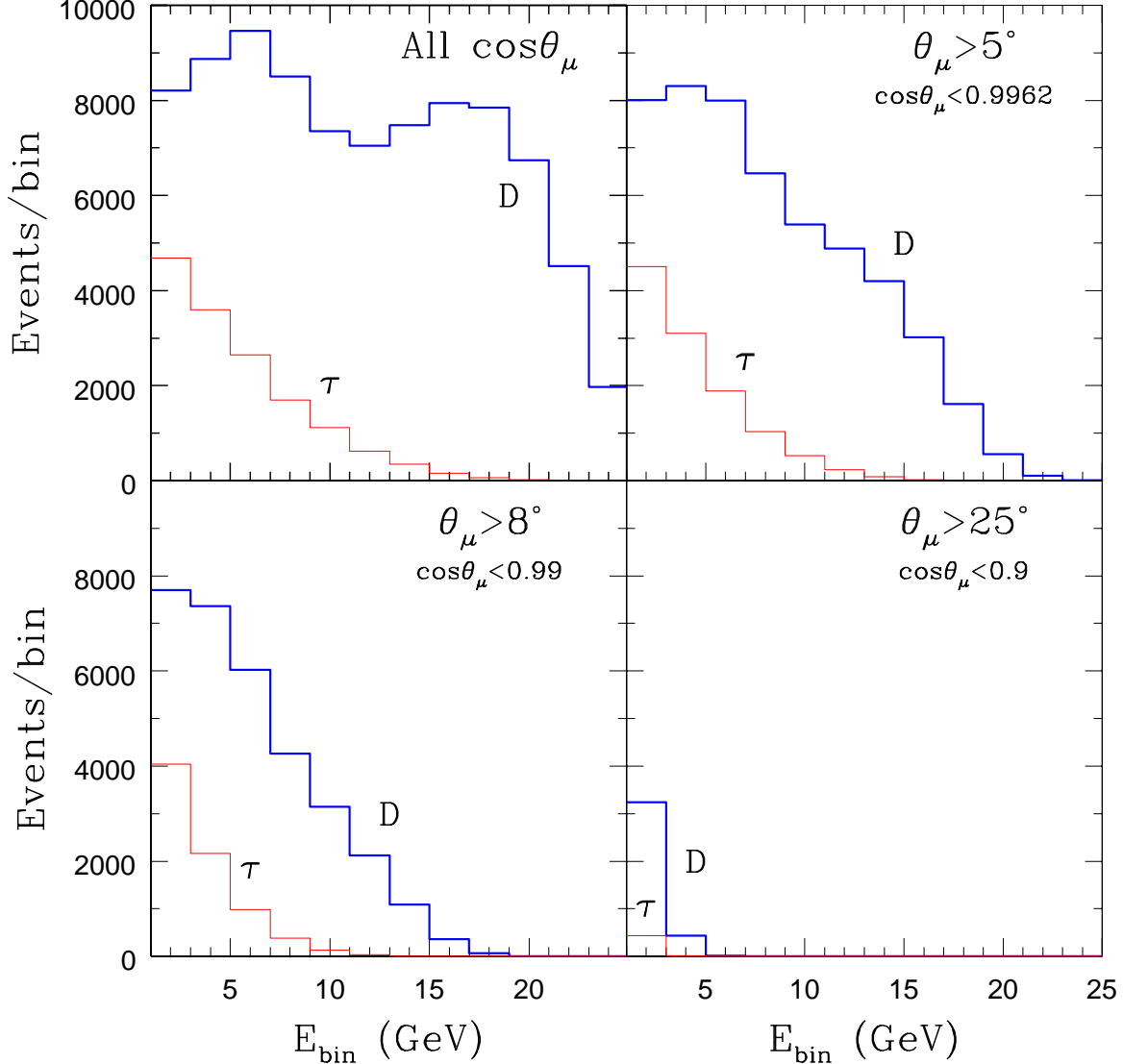


FIG. 7: Effects of angular cuts on the tau contribution to muon events at neutrino factories. For details, see the text. It may not be possible to devise effective cuts to remove the tau contribution which must therefore be included in any analysis.

large uncertainties inherent in any perturbative QCD calculation at low/medium  $Q^2$ , these are compounded for the case of the heavy tau where mass corrections are large. Furthermore, since these contributions result from oscillations, no near detector can help reduce the uncertainties more. Hence overall uncertainties are much larger for the tau contribution than for direct muons and this exacerbates the problem of precision measurements with tau contamination.

We now proceed to show this effect through specific numerical calculations. We use a combined overall normalization error of 0.1% for direct muon events (separate flux and cross-section normalization errors are not required as for WS studies since the RS events are by far the dominant contribution and errors are kept well in check by studies at the near detector as described above).



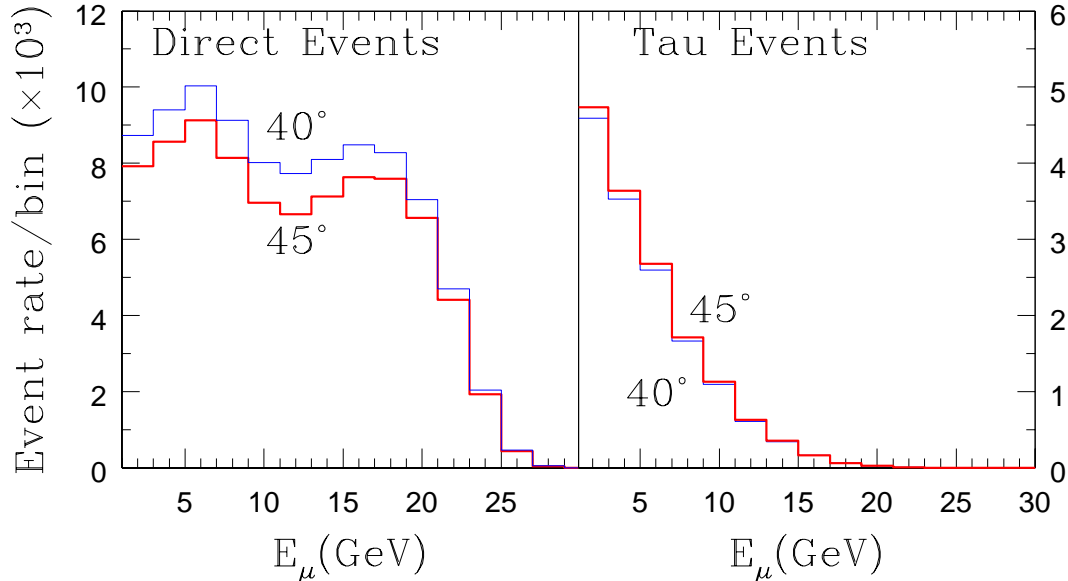


FIG. 8: Variation of direct and tau induced muon events with  $\theta_{23}$ . While increase in  $\theta_{23}$  decreases the direct muon events, those coming from production and decay of taus tend to increase marginally with larger  $\theta_{23}$ . The conflicting behavior results in less sensitivity in the total events.

We use a modest normalization error of 2% for the total (direct+tau) events; since the same (muon neutrino) flux contributes, this is essentially the error on the ratio of the tau to muon cross-sections. We use typical input values of  $(\Delta m^2, \theta_{23}, \theta_{13})$  to estimate how well the generated “data” can be fitted, and calculate the resulting precision on the parameters. Again, we keep the solar parameters fixed at their best-fit values and set  $\delta_{CP}$  to zero. The best fits (and regions of confidence levels in parameter space) are obtained by minimizing the chi-squared according to the method of “pulls” [26] :

$$\chi^2 = \min_{\xi} \left[ \sum_{\text{bin}=1}^N \frac{(\overline{\mathcal{R}}_{\text{bin}}^{th}(\xi) - \mathcal{R}_{\text{bin}}^{data})^2}{\sigma_{\text{bin}}^2} + \xi^2 \right]. \quad (8)$$

Here the normalization uncertainty for the event rate in a bin is parameterized as a linear function of the pull:

$$\overline{\mathcal{R}}_{\text{bin}}^{th}(\xi) = \mathcal{R}_{\text{bin}}^{th} (1 + \Delta N \xi), \quad (9)$$

where  $\Delta N$  is either 0.1 or 2% for direct and total respectively and  $\xi$  is the pull that accounts for the overall systematic error on the rate. While the expression can be minimized over a set of pulls for each systematic error, this is not needed since the rate is dominated by the RS events as explained earlier. Here the theoretical rates in a bin correspond to a central value of  $\xi = 0$  with  $\xi = \pm 1$  representing  $1\sigma$  errors. We follow the prescription of Ref. [26], where the chi-squared is first minimized over  $\xi$  and then minimized with respect to oscillation parameters to get the best-fit values and regions.

### E. Deviation of $\theta_{23}$ from maximality

We present results for a typical sample set of input parameters,  $(\Delta m^2, \theta_{23}, \theta_{13} = 2.4 \times 10^{-3} \text{ eV}^2, 41.9^\circ, 1^\circ)$ . After minimizing over the pull, we minimize over  $\Delta m^2$  and  $\theta_{23}$ , keeping the 13 mixing

angle fixed. Fig. 9 shows the allowed region in  $\Delta m^2$ - $\theta_{23}$  parameter space at 99% CL ( $\Delta\chi^2 = 9.21$ ). The solid line correspond to considering direct muon events alone and the dashed line correspond to using the total events, including those from tau decay.

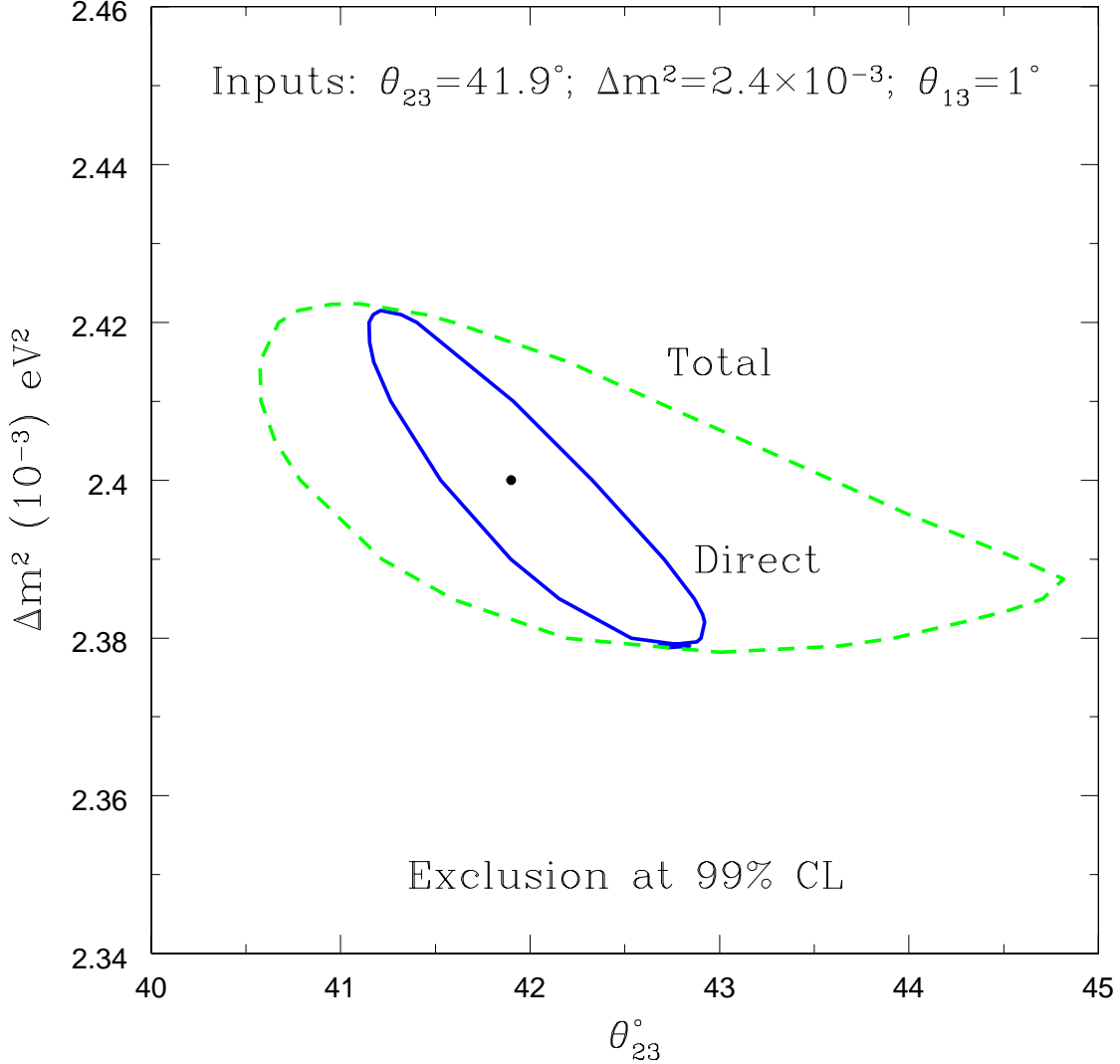


FIG. 9: Allowed parameter space in  $\Delta m^2$ - $\theta_{23}$  space at 99% CL from CC events directly producing muons (solid line) and with the inclusion of muons from tau decay as well (dashed line) for input parameter values of  $(\Delta m^2, \theta_{23}, \theta_{13} = 2.4 \times 10^{-3} \text{ eV}^2, 41.9^\circ, 1^\circ)$ .

Note that the selected signal (all muons in the final state, independent of charge) is dominated by RS muons and is therefore insensitive to the *octant* of  $\theta_{23}$  as well as the *sign* of  $\Delta m^2$  (or the mass hierarchy). These can be probed only through a study of WS muons, as has been discussed elsewhere. Returning to the issue of deviation of  $\theta_{23}$  from maximality, it can be seen that the 99% CL contour is much more constrained with direct muons than for total muons, including those from tau decay. In particular, it is the  $\Delta m^2$  values that are smaller than the input (true) value, that broaden the contour and limit the discrimination. Hence the effect of adding in the tau contribution is a worsening in the precision with which  $\theta_{23}$  and its deviation from maximality can be measured: a spread of  $\sim 2^\circ$  if tau events are removed and  $\sim 4.5^\circ$  when they are included. This occurs because of the conflicting dependence on  $\theta_{23}$  of the two contributions, as has been discussed earlier. However, it can be seen from Fig. 9 that the inclusion of the tau events does not affect the determination of

(the modulus of)  $\Delta m^2$  which is tightly constrained to better than 1% in either case.

The largest true value of  $\theta_{23}$  that can be discriminated from maximal through a study of muon events in neutrino factories is shown in Fig. 10, as a function of  $\Delta m^2$ . Again,  $\theta_{13}$  is kept fixed at  $\theta_{13} = 1^\circ$ . While there is a distinct but mild dependence on  $\Delta m^2$ , it is seen that tau contamination worsens the ability to discriminate  $\theta_{23}$  from maximal, thus making this measurement as well as an octant measurement harder than originally expected.

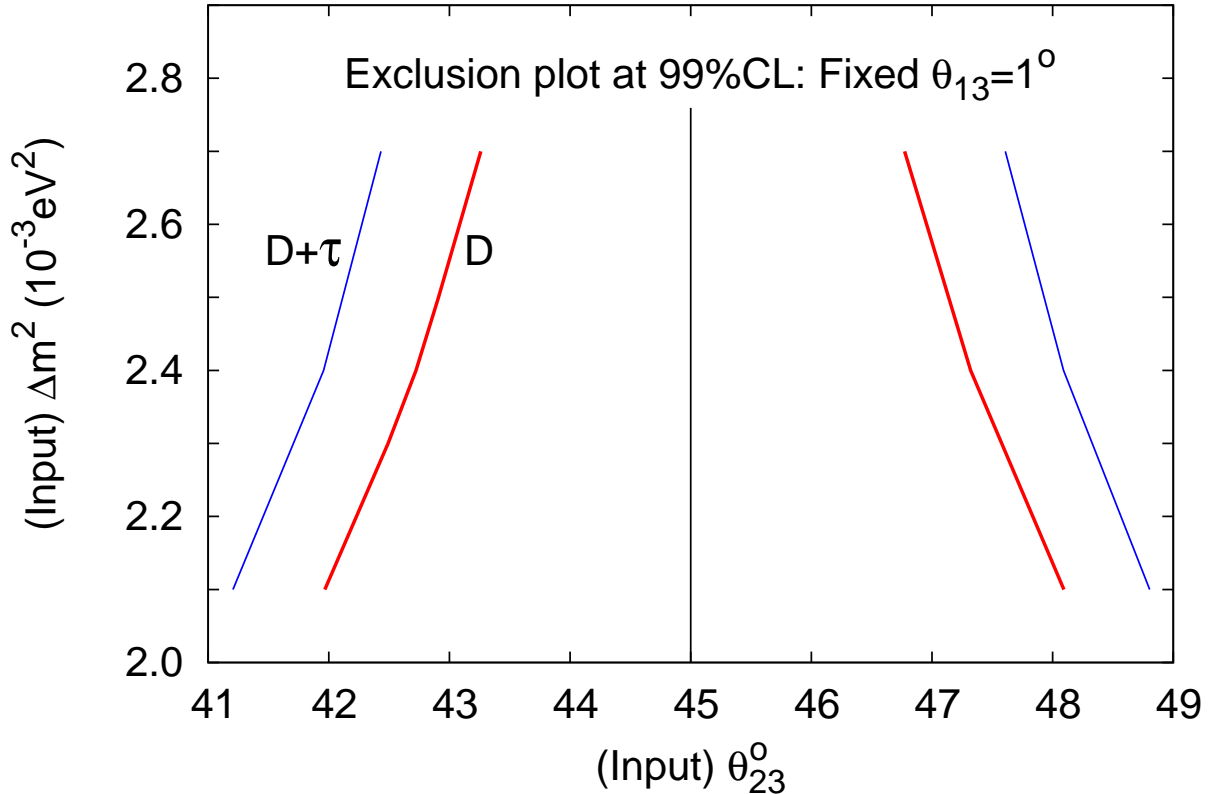


FIG. 10: The figure shows the largest (smallest) true value of  $\theta_{23}$  in the first (second) octant that can be discriminated from a maximal value of  $\theta_{23} = \pi/4$  as a function of  $\Delta m^2$  when only Direct ( $D$ ) and total ( $D + \tau$ ) events are considered. Here  $\theta_{13}$  is kept fixed:  $\theta_{13} = 1^\circ$ .

### F. Effect of $\theta_{13}$

Due to the extraordinarily large RS signal, it is anticipated that some of the early measurements at a neutrino factory will be those of precision determination of  $\Delta m^2$  and  $\theta_{23}$  and the deviation of the latter from maximality. Certainly a strong case for conventional neutrino factories of the type considered here will be made only when  $\theta_{13}$  is small, below the reach of near-future super-beams or reactor searches. Hence we expect  $\theta_{13}$  to be relatively unknown at the time of such measurements, typically restricted to a value  $\theta_{13} < 2^\circ$  ( $\sin^2 2\theta_{13} < 0.005$ ). The uncertainty in  $\theta_{13}$  will worsen the allowed parameter space from both direct and total muon events. In particular, the dependence of the event rates (both direct and tau-induced) is such that values of  $\theta_{13}$  larger than the true value lower the  $\chi^2$  near maximal  $\theta_{23}$ , and hence worsen the power of discriminating against it. In other

words, the tighter the upper bound on  $\theta_{13}$ , better will be the discrimination of  $\theta_{23}$  from maximality. This can be seen from Fig. 11 where the chi-squared is plotted (for a fixed normalization,  $\xi = 0$ , for clarity) for two different  $\Delta m^2$  values, for the same input set as before.

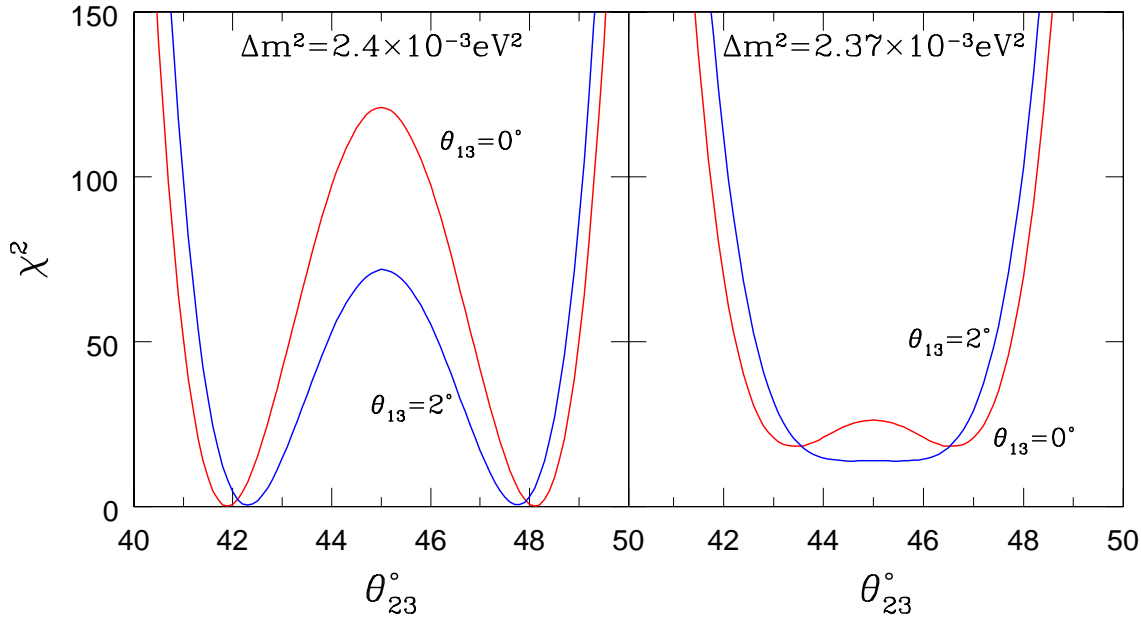


FIG. 11: Effect of  $\theta_{13}$  on  $\chi^2$  for input parameter values of  $(\Delta m^2, \theta_{23}, \theta_{13} = 2.4 \times 10^{-3} \text{ eV}^2, 41.9^\circ, 1^\circ)$ . Increase in  $\theta_{13}$  lowers the  $\chi^2$  near maximality, and hence worsens the power of discriminating against it, as shown for two typical values of  $\Delta m^2$ , for the same input parameter values.

The effect again leads to a widening of the contour in regions where  $\Delta m^2$  is smaller than the true value, as can be seen from Fig. 12. Here, the normalization is kept fixed to  $\xi = 0$  for clarity in understanding the effect of varying  $\theta_{13}$  and we have assumed a bound  $\theta_{13} < 2^\circ$ , with the contour corresponding to allowed parameter values at 99% CL. Fig. 12 also shows, for completeness, the false minima in the second octant and in both octants with the inverted hierarchy. Similar results are obtained if the true  $\theta_{23}$  is in the second octant and/or the hierarchy is inverted, although the precision is marginally worse when the true  $\theta_{23}$  is in the second octant.

Alternately, we can allow  $\theta_{13}$  to vary freely, but include a prior on this parameter, through an additional term in the chi-squared to include the expected bound on  $\sin^2 2\theta_{13}$  [27] from upcoming experiments,

$$\chi^2 \rightarrow \chi^2 + \frac{(\sin^2 2\theta_{13} - \sin^2 2\theta_{13}^{\text{true}})^2}{\sigma_{13}^2}, \quad (10)$$

where  $\sigma_{13}$  is the error on  $\sin^2 2\theta_{13}^{\text{true}}$  which we take to be  $\sigma_{13} = 0.005$ . Using this modified definition of the chi-squared, and the same procedure as before, the 99% CL contours in the parameter space now correspond to  $\Delta\chi^2 = 11.36$  for 3 parameters,  $\Delta m^2$ ,  $\theta_{23}$  and  $\theta_{13}$ . In Fig. 13 we show the largest true value of  $\theta_{23}$  that can be discriminated from maximal when both  $\Delta m^2$  and  $\theta_{13}$  are varied, as a function of the true  $\Delta m^2$ , given the normalization uncertainties as specified earlier. The inclusion of tau events still worsens the measurement, although the situation is not as acute as when  $\theta_{13}$  was kept fixed. Again, there is better discrimination for larger  $\Delta m^2$ .

*c. Some miscellaneous remarks* : We note that the ability to discriminate from maximality is marginally asymmetric between the two octants when  $\theta_{13}$  is different from zero, as is the case

in all the examples shown. The results are better if the true value lies in the first octant but not significantly so. Furthermore, the discrimination capability improves as the uncertainty  $\sigma_{13}$  decreases. Finally, there is a non-trivial dependence of the results on the muon beam energy,  $E_b$ . While the event rate increases with  $E_b$ , the number of “useful” events does not, since the sensitivity to mixing parameters is best for intermediate neutrino energies,  $E_\nu \sim 5\text{--}10$  GeV. This arises from the energy dependence of the oscillation probabilities as well as the energy dependence of Earth matter effects. It appears that muon beams with energies 15–25 GeV are best suited for such measurements.

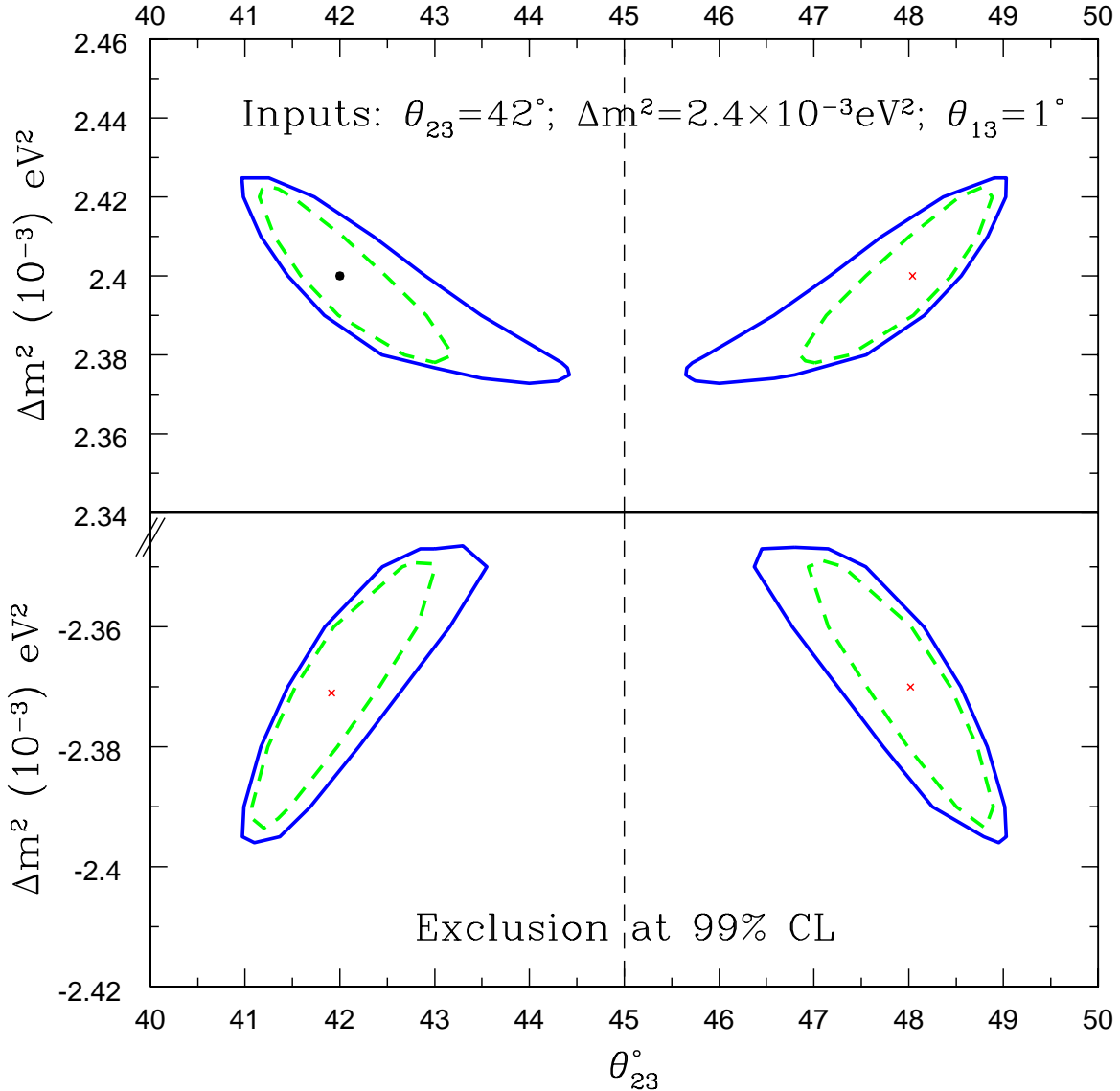


FIG. 12: Allowed parameter space in  $\Delta m^2\text{--}\theta_{23}$  space at 99% CL from all CC events producing muons, including tau events, with a fixed normalization ( $\xi = 0$ ). The dashed lines corresponds to fits with a fixed  $\theta_{13} = 1^\circ$  and the solid lines result from varying  $\theta_{13}$  with  $0 < \theta_{13} < 2^\circ$ . The input parameter values are  $(\Delta m^2, \theta_{23}, \theta_{13} = 2.4 \times 10^{-3} \text{eV}^2, 42.0^\circ, 1^\circ)$ . For completeness, the contours in the second octant as well as with the inverted hierarchy are shown.

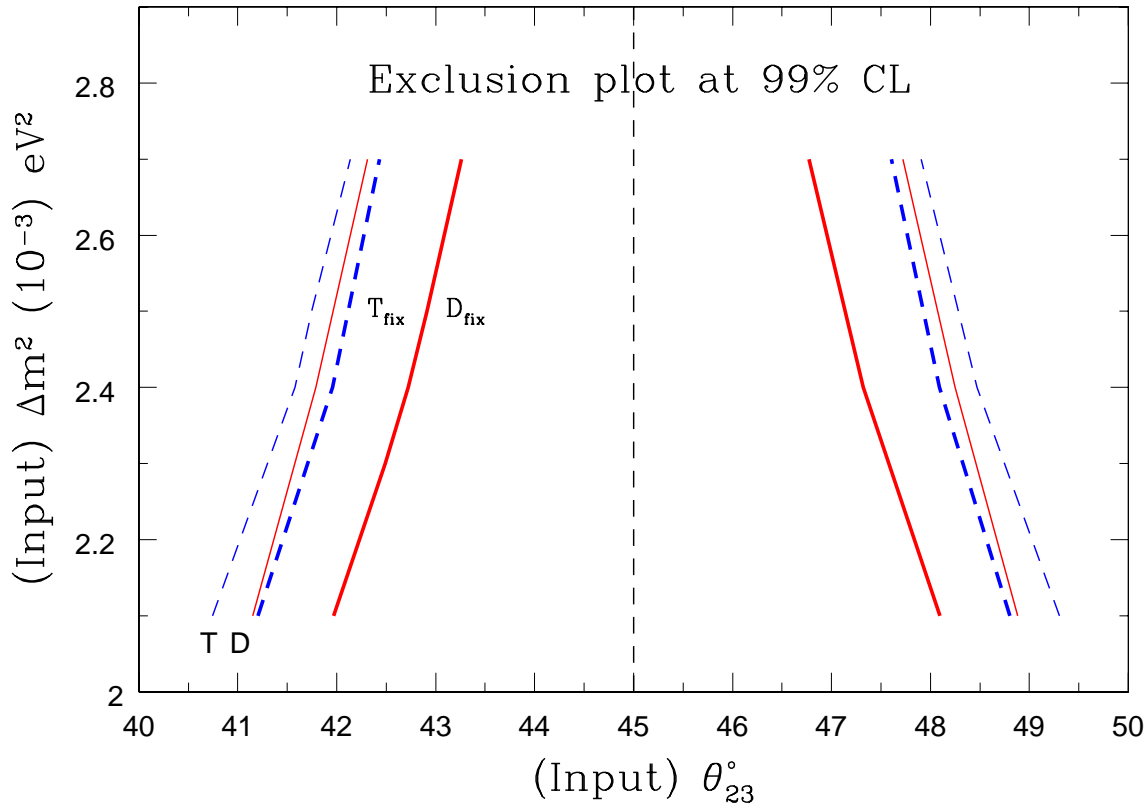


FIG. 13: The largest (smallest) true value of  $\theta_{23}$  in the first (second) octant that can be discriminated from a maximal value of  $\theta_{23} = \pi/4$  as a function of the true  $\Delta m^2$  when uncertainties in  $\Delta m^2$ ,  $\theta_{13}$  and the normalization are taken into account. All the analyses use an input value of  $\theta_{13} = 1^\circ$ . The solid (dashed) lines are for direct muon events only (total = direct + tau). The lighter obtained with an uncertainty of  $\sigma_{13} = 0.005$  on  $\sin^2 2\theta_{13}$  will approach the darker curves corresponding to fixed  $\theta_{13}$  as the uncertainty on  $\theta_{13}$  decreases.

## V. CONCLUSION

We have re-examined the precision to which the leading atmospheric parameters can be measured at a standard neutrino factory. We have addressed the little-studied issue of contamination of the (right or wrong sign) muon events sample due to oscillations of the muon or electron neutrinos (anti-neutrinos) to tau neutrinos (anti-neutrinos). These, through charge current interactions in the detector result in tau leptons, which can then decay to muons, adding to the right as well as wrong sign muon events obtained directly, without tau production. The tau contribution *worsens* the precision to which  $\theta_{23}$  can be measured while leaving the determination of the atmospheric mass squared difference  $|\Delta m^2|$  unchanged. Hence the tau contamination worsens the ability to discriminate against maximal  $\nu_\mu \leftrightarrow \nu_\tau$  mixing. Any cuts imposed to remove the tau events drastically reduce the events from direct muon production as well and are hence impracticable. Uncertainties from this tau background have therefore first to be brought under control before making precision parameter measurements at neutrino factories.

## Appendix A

We detail the kinematics of neutrino–nucleus CC interactions with muons in the final state (direct muon events) and that of CC interactions with tau in the final state with subsequent tau decay into muons in the lab frame (tau-induced muon events). The events are characterized by the final muon energy and direction, i.e., the entire muon spectrum. Hence the detailed kinematics of the interactions, both for direct muon production and via tau decay, are required.

We define the four-momenta of the incoming neutrino ( $k$ ), target nucleon ( $p$ ), produced  $\tau$  lepton ( $k'$ ) and the muon ( $q_1$ ) coming from the decay of the tau in the laboratory frame as,

$$\begin{aligned} k &= (E_\nu, 0, 0, E_\nu) , \\ p &= (M, 0, 0, 0) , \\ k' &= (E_\tau, p_\tau \sin \theta_\tau, 0, p_\tau \cos \theta_\tau) , \\ q_1 &= (E_\mu, p_\mu \sin \theta_\mu \cos \phi_\mu, p_\mu \sin \theta_\mu \sin \phi_\mu, p_\mu \cos \theta_\mu) , \end{aligned} \quad (11)$$

where  $M$  is the (isoscalar) nucleon mass. The kinematics is standard and straightforward for the case of  $\nu_\mu$  interactions (where there is no tau production, all components of  $k'$  are zero), with the angles of the direct muon produced in the CC interaction taking values  $0 < \cos \theta_\mu < 1$  and  $\phi_\mu = 0$ .

The threshold for the interaction is given by  $E_\nu^{\text{thr}} = m_l + m_l^2/2M$ , for  $l = \mu, \tau$ ; hence it is significant,  $E_\nu \gtrsim 3.5$  GeV, in the case of tau production. Furthermore, in the case of  $\nu_\tau$  interactions, the tau is produced at a very forward angle,  $c_{\min} < \cos \theta_\tau < 1$ , in the lab frame, where

$$c_{\min}(E_\nu) = \sqrt{1 + \frac{M}{E_\nu} + \frac{M^2}{E_\nu^2} - \frac{m_\tau^2}{4E_\nu^2} - \frac{M^2}{m_\tau^2}} . \quad (12)$$

Finally, the angle  $\phi_\mu$  of the muon produced during tau decay is restricted by the decay kinematics to obey the constraint:

$$\cos \phi_\mu > \frac{2(E_\mu E_\tau - p_\mu p_\tau \cos \theta_\tau \cos \theta_\mu) - (m_\tau^2 + m_\mu^2)}{2p_\mu p_\tau \sin \theta_\tau \sin \theta_\mu} . \quad (13)$$

In addition, the available phase space in both direct muon production and tau-induced muon production, restricts the available lepton energy to  $E_- < E_l < E_+$ , where  $l = \mu, \tau$ . We have,

$$E_\pm(E_\nu, \cos \theta_l) = \frac{1}{2a}(b \pm \sqrt{b^2 - 4ac}) , \quad (14)$$

with

$$\begin{aligned} a &= (E_\nu + M)^2 - E_\nu^2 \cos^2 \theta_l , \\ b &= (E_\nu + M)(2ME_\nu + m_l^2) , \\ c &= m_l^2 E_\nu^2 \cos^2 \theta_l + (ME_\nu + m_l^2/2)^2 . \end{aligned} \quad (15)$$

At the limits,  $m_X = m_{X,\min} = M$ , the nucleon mass. The notation is standard:  $m_X^2 = W^2 = (p + q)^2$ , where  $q = k' - k$  is the 4-momentum of the intermediate gauge boson in the lab frame;  $m_X$  is constrained to lie in the range  $\sqrt{s} - m_l \geq m_X \geq M$ , with  $s = (k + p)^2$ .

The expression for semi-leptonic decay,  $\tau \rightarrow \mu \nu_e$ , of a tau into a final state muon, with four-momenta  $k'$  and  $q_1$  respectively (defined in Eq. (11)), in the lab frame of the original neutrino–nucleon interaction, is given by,

$$\frac{d\Gamma(E_\tau, E_\mu, \theta_\tau, \theta_\mu, \phi_\mu)}{dE_\mu d\cos \theta_\mu d\phi_\mu} = G_F^2 \frac{p_\mu}{48E_\tau \pi^4} \left[ 3(m_\tau^2 + m_\mu^2)(k' \cdot q_1) - 4(k' \cdot q_1)^2 - 2m_\tau^2 m_\mu^2 \right] . \quad (16)$$

The total decay width of the tau is  $\Gamma_\tau = 1/c\tau$  where  $c\tau = E_\tau/m_\tau(c\tau_0)$  where the rest-frame lifetime is  $c\tau_0 = 87.2$  microns.

**Acknowledgments:** We thank M.V.N. Murthy for discussions and a careful reading of the manuscript. One of us (NS) thanks Murthy for suggesting a study of precision measurements at neutrino factories.

- 
- [1] B. Pontecorvo, J. Exp. Theor. Phys. **33**, 549 (1957); Sov. Phys. JETP, **6**, 429 (1958); Z. Maki, M. Nakagawa and S. Sakata, Prog. Theor. Phys. **28**, 870 (1962).
- [2] S.N. Ahmed et al. (SNO Collaboration), Phys. Rev. Lett. **92**, 181301 (2004) [ArXiv:nucl-ex/0309004]; Q.R. Ahmad, et al. (SNO Collaboration), Phys. Rev. Lett. **89**, 011302 (2002); Phys. Rev. Lett. **89**, 0113010 (2002), Phys. Rev. Lett. **87**, 071301 (2001); S. Fukuda, et al. (Super-Kamiokande Collaboration), Phys. Lett. **B 539**, 179 (2002), Phys. Rev. Lett. **86**, 5656 (2001); Phys. Rev. Lett. **86**, 5651 (2001); Fukuda, Y. et al. (Super-Kamiokande Collaboration), Phys. Rev. Lett. **82**, 2430 (1999); Phys. Rev. Lett. **82**, 1810 (1999); Phys. Rev. Lett. **81**, 1158 (1998); W. Hampel, et al. (GALLEX Collaboration), Phys. Lett. **B 447**, 127 (1999); J.N.Abdurashitov, et al. (SAGE Collaboration), Phys. Rev. Lett. **83**, 4686 (1999); K.S. Hirata, et al. (Kamiokande-II Collaboration), Phys. Rev. **D 44**, 2241 (1991); R. Davis, (Homestake) Prog. Part. Nucl. Phys. **32**, 13 (1994).
- [3] Y. Ashie et al. (Super-Kamiokande Collaboration), Phys. Rev. Lett. **93**, 101801 (2004); M. Ishitsuka (Super-Kamiokande Collaboration), NOON2004, The 5th Workshop on "Neutrino Oscillations and their Origin", 11-15 February 2004, Tokyo, Japan; Y. Ashie et al. (Super-Kamiokande Collaboration), Phys. Rev. **D 71**, 112005 (2005); Y.Fukuda, et al.(Super-Kamiokande Collaboration), Phys. Rev. Lett. **81**, 1562 (1998); G. Giacomelli et al. (MACRO Collaboration), Nucl. Phys. Proc. Suppl. **145** 116 (2005); W.W.M. Allison et al. (Soudan-2 Collaboration), Phys. Rev. **D 72**, 052005 (2005); also see Phys. Rev. **D 68**, 113004 (2003); D. Casper et al. (IMB-3 Collaboration), Phys. Rev. Lett. **66**, 2561 (1991).
- [4] K. Eguchi et al. (KamLAND Collaboration), Phys. Rev. Lett. **90**, 021802 (2003); Apollonio, M. et al. (CHOOZ Collaboration), Eur. Phys. J. **C 27**, 331 (2003).
- [5] M.H. Ahn, et al. (K2K Collaboration), Phys. Rev. Lett. **90**, 041801 (2003).
- [6] P. Adamson et al. (MINOS Collaboration) Phys. Rev. **D73**, 072002 (2006).
- [7] Some of the older studies are found in, for instance, V. Barger, S. Geer, R. Raja, K. Whisnant, Phys.Rev. **D 62**, 013004 (2000) [ArXiv:hep-ph/9911524]; A. Cervera, A. Donini, M. B. Gavela, J. J. Gomez Cadenas, P. Hernandez, O. Mena and S. Rigolin, Nucl. Phys. **B 579**, 17 (2000) [Erratum-ibid. **B 593**, 731 (2001)]; P. Huber, M. Lindner, M. Rolinec, W. Winter, Phys.Rev. **D 74**, 073003 (2006) and references therein. See also the IDS physics studies in Ref. [8] below.
- [8] For general reviews on neutrino factory parameters, see A. Bandyopadhyay *et al.* [ISS Physics Working Group], Rept. Prog. Phys. **72**, 106201 (2009) [arXiv:0710.4947 [hep-ph]].
- [9] P.F. Harrison, D. H. Perkins and W. G. Scott, Phys. Lett. **B 349**, 137, 1995; *ibid.* **B 530**, 167 (2002) [ArXiv:hep-ph/0202074]; E. Ma and G. Rajasekaran, Mod. Phys. Lett. **A 16**, 2207 (2001) [ArXiv:hep-ph/0109236]; V.D. Barger, S. Pakvasa, T.J. Weiler and K. Whisnant, Phys. Lett. **B 437**, 107, 1998, [ArXiv:hep-ph/9806387]; G. Altarelli and F. Feruglio, JHEP **9811**, 021 (1998) [ArXiv:hep-ph/9809596]; for some more recent papers see for example, Z. z. Xing, H. Zhang and S. Zhou, Phys. Lett. **B 641**, 189 (2006) [arXiv:hep-ph/0607091]; K. S. Babu and X. G. He, arXiv:hep-ph/0507217; R. N. Mohapatra and W. Rodejohann, Phys. Rev. **D**



- 72**, 053001 (2005) [arXiv:hep-ph/0507312].
- [10] K. Hagiwara, K. Mawatari and H. Yokoya, Nucl. Phys. **B 668**, 364 (2003) [Erratum-ibid. **B 701**, 405 (2004)] [arXiv:hep-ph/0305324]; M. Aoki, K. Hagiwara, K. Mawatari and H. Yokoya, Nucl. Phys. **B 727**, 163 (2005) [arXiv:hep-ph/0503050].
- [11] D. Indumathi, M.V.N. Murthy, G. Rajasekaran, Nita Sinha, Phys. Rev. **D 74**, 053004 (2006) [ArXiv:hep-ph/0603264].
- [12] M.C. Gonzalez-Garcia and Y. Nir, Rev. Mod. Phys. **75**, 345 (2003) [ArXiv:hep-ph/020205].
- [13] D. Indumathi and M.V.N. Murthy, Phys. Rev. **D 71**, 013001 (2005) [ArXiv:hep-ph/0407336].
- [14] G.L. Fogli, E. Lisi, A. Marrone, A. Palazzo, Prog.Part.Nucl.Phys. **57**,742 (2006) [ArXiv:hep-ph/0506083].
- [15] A.M. Dziewonski and D.L. Anderson, Preliminary reference Earth model (PREM), Phys. Earth Plan. Int. **25**, 297 (1981).
- [16] Thomas Schwetz, Mariam Tortola, Jose W.F. Valle, New J. Phys. **10** 113011 (2008) [ArXiv:0808.2016].
- [17] IDS-NF baseline study, IDS-NF-Baseline-2007/1.0, prepared by the IDS-NF Steering Group, Nov 2008.
- [18] See, for instance, C. Crisan and S. Geer, Fermilab-TM-2101; A. Broncano and O. Mena, Eur. Phys. J. **C 29**, 197 (2003) [ArXiv:hep-ph/0203052] and Ref. [8].
- [19] W. Furmanski and R. Petronzio, Z. Phys. **C 11**, 293 (1982).
- [20] H. Georgi and H.D. Politzer, Phys. Rev. **D 14**, 1829 (1976).
- [21] S. Kretzer and M.H. Reno, Phys. Rev. **D 69**, 034002 (2004) [ArXiv:hep-ph/0307023]; Phys. Rev. **D 66**, 113007 (2002) [ArXiv:hep-ph/0208187].
- [22] D. Schmitz, Invited talk at NuFact09, 11th International Workshop on Neutrino Factories, Super-beams and beta-beams, Chicago, July 2009.
- [23] A. Para, Acta Phys. Polon. **B 31**, 1313 (2000) [ArXiv:hep-ph/0005012]; C. Andreopoulos, P. Stamoulis and G. Tzanakos, NuMI-Note-ATM\_NU-990, UA/ Phys/ HEP/ 11-05-2003 (<http://www-numi.fnal.gov/>).
- [24] D. Indumathi (INO Collaboration), Proc. 29th International Conf. on Cosmic Rays, ICRC, Pune, **Vol 10**, 199 (2005); (<http://www.imsc.res.in/~ino>).
- [25] P. Huber and W. Winter, Phys. Rev. **D 68** 037301 (2003) [ArXiv:hep-ph/0301257].
- [26] M.C. Gonzalez-Garcia and M. Maltoni, Phys. Rev. **D 70**, 033010 (2004).
- [27] Typical bounds at 90% CL expected from reactor experiments on  $\sin^2 2\theta_{13}$  are 0.03 (from Double CHOOZ, Fumihiko Suekane, Proceedings for TIPP09, ArXiv:0906.1639); 0.01 (from Daya Bay, M.-C. Chu, ICHEP08 Proceedings, ArXiv:0810.0807), that from T2K varies between  $\sin^2 2\theta_{13} \sim 0.008\text{--}0.02$  (N. C. Hastings, talk at Heavy Quarks and Leptons, Melbourne, 2008), ArXiv:0905.1211; P. Huber, M. Lindner, T. Schwetz and W. Winter, arXiv:0907.1896 [hep-ph]; see also Ref. [8].